Biomacromolecule-biomacromolecule interactions as probed by NMR spectroscopy

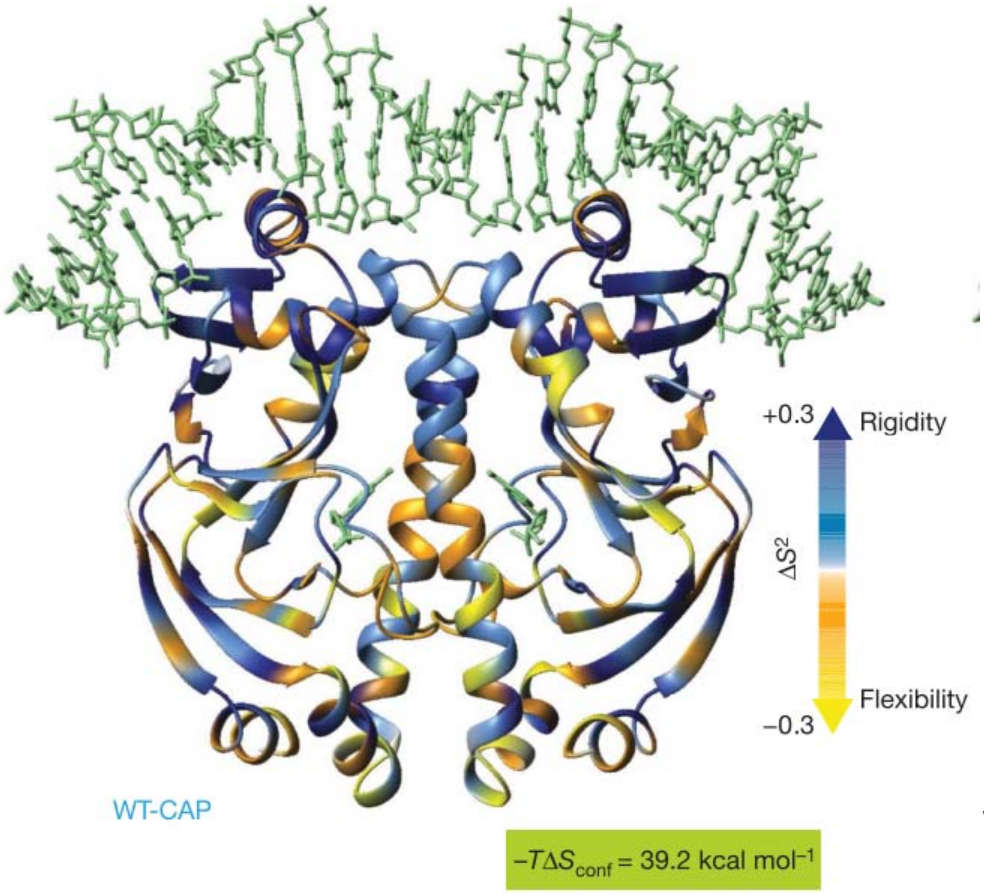

Tzeng, S.-R. & Kalodimos, C. G. Dynamic activation of an allosteric regulatory protein. Nature 462, 368–72 (2009).

W. Milo Westler
Bchm/Chm 872
“Selected Topics in Macromolecular and Biophysical Chemistry”
Spring 2013

Protein Structure Determination

Ubiquitin

MQIFVKTLTGKTITLEVEPSDTIENVKAKIQDKEGIPPD
QQRLIFAGKQLEDGRTLSDYNIQKESTLHLVLRLRGG

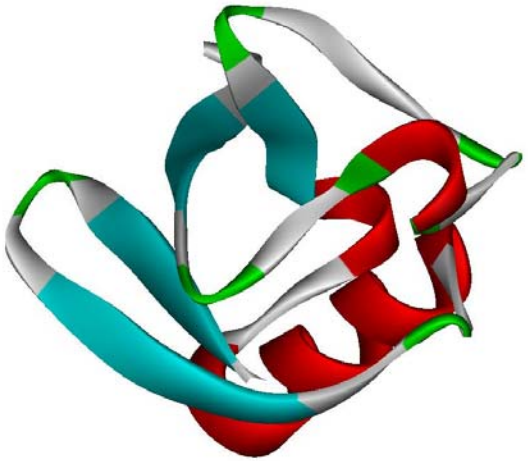

With apologies to Staples

Ubiquitin

MQIFVKTLTGKTITLEVEPSDTIENVKAKIQDKEGIPPD
QQRLIFAGKQLEDGRTLSDYNIQKESTLHLVLRLRGG

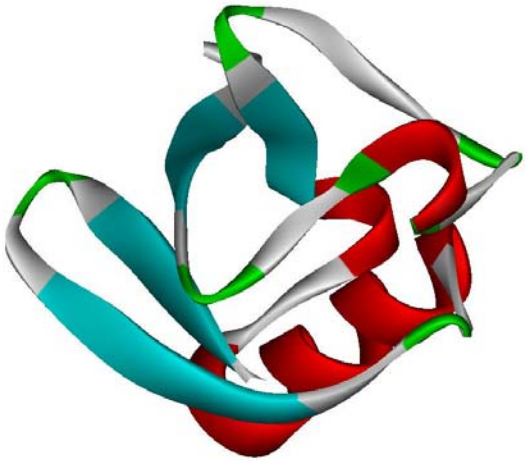

Ubiquitin

MQIFVKTLTGKTITLEVEPSDTIENVKAKIQDKEGIPPD
QQRLIFAGKQLEDGRTLSDYNIQKESTLHLVLRLRGG

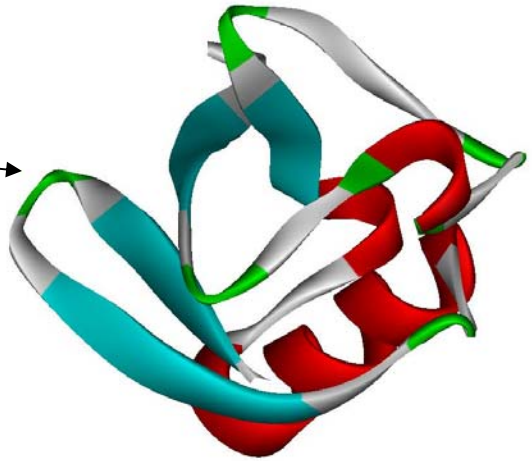

Overview of structure determination

- **Backbone assignments (H, N, C^{α}, C^{β}, and C') {we know the sequence!}**
- **Sidechain assignments – rest of carbons and protons**
- **NOE constraints**

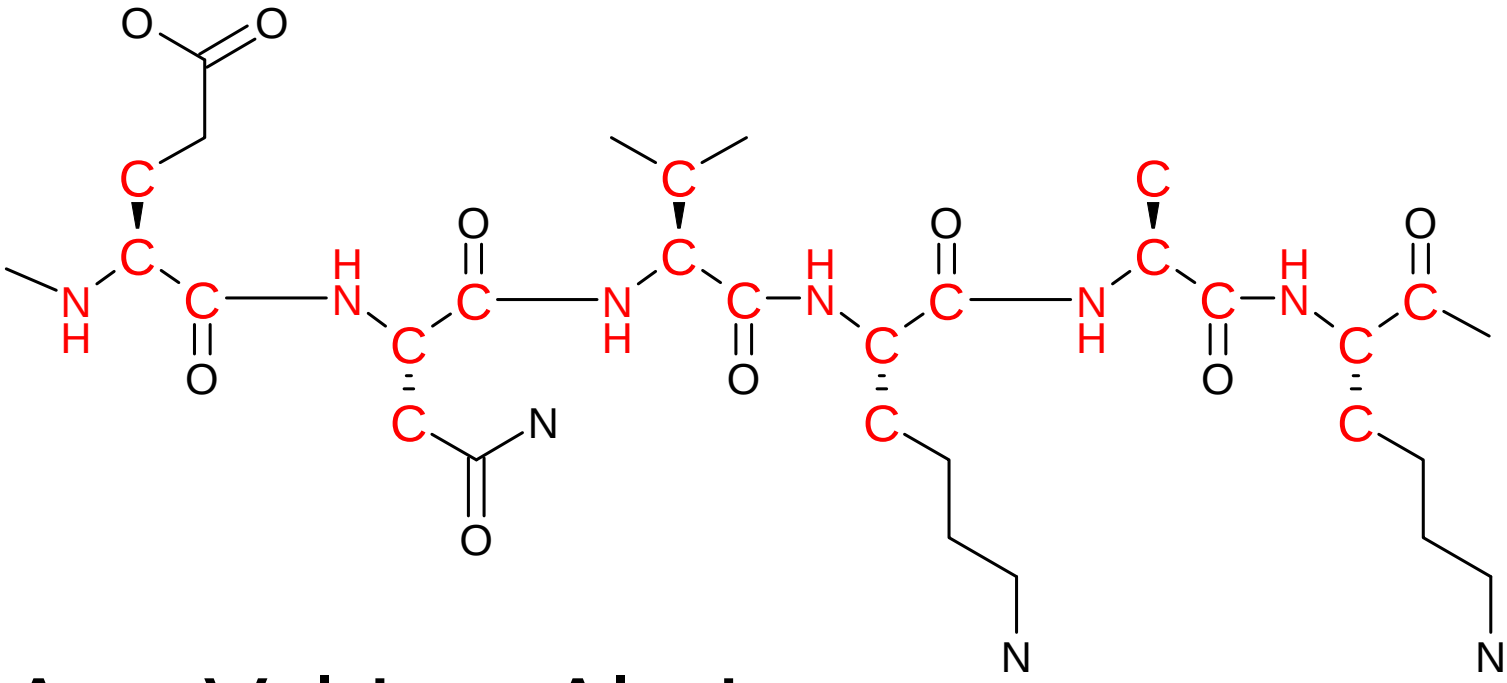

Glu-Asn-Val-Lys-Ala-Lys

Overview of structure determination

- Backbone assignments (H, N, C^{α}, C^{β}, and C')
- **Sidechain assignments – rest of carbons and protons**
- NOE constraints

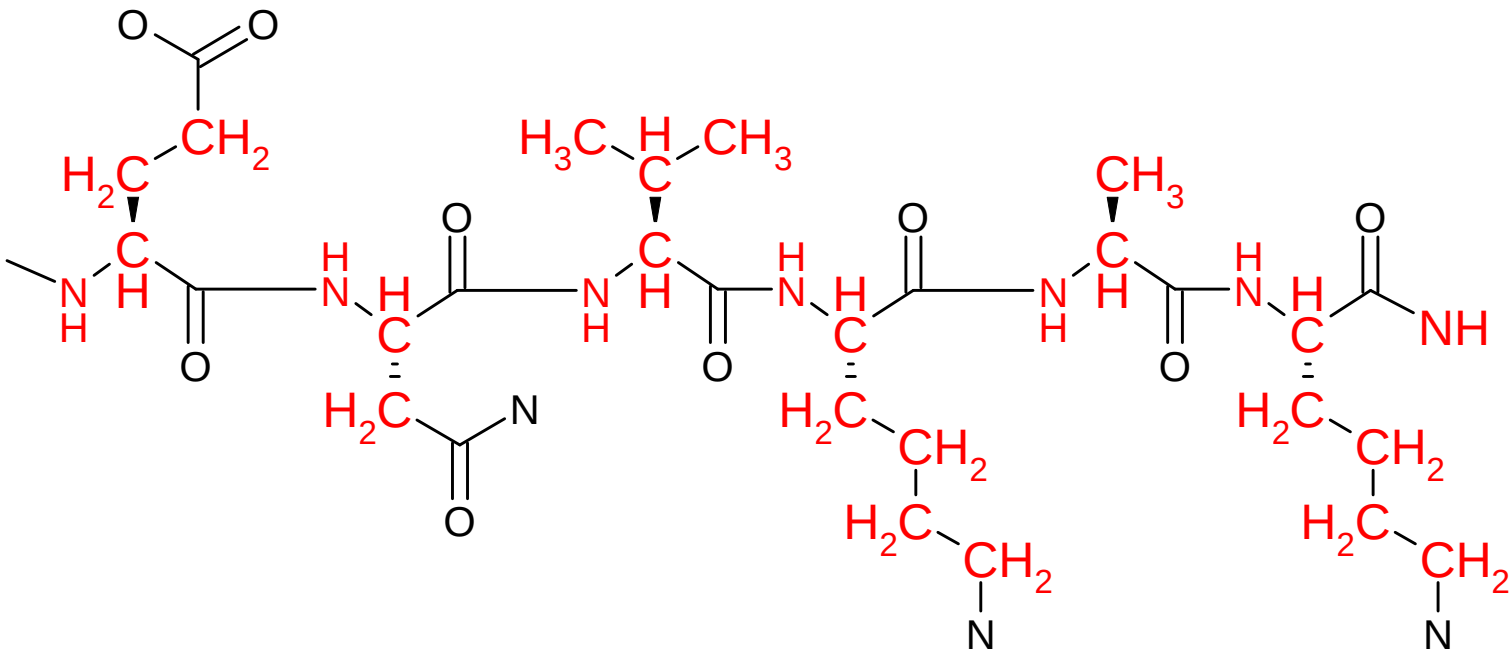

Overview of structure determination

- Backbone assignments (H, N, C^{α}, C^{β}, and C')
- Sidechain assignments – rest of carbons and protons
- **NOE constraints**

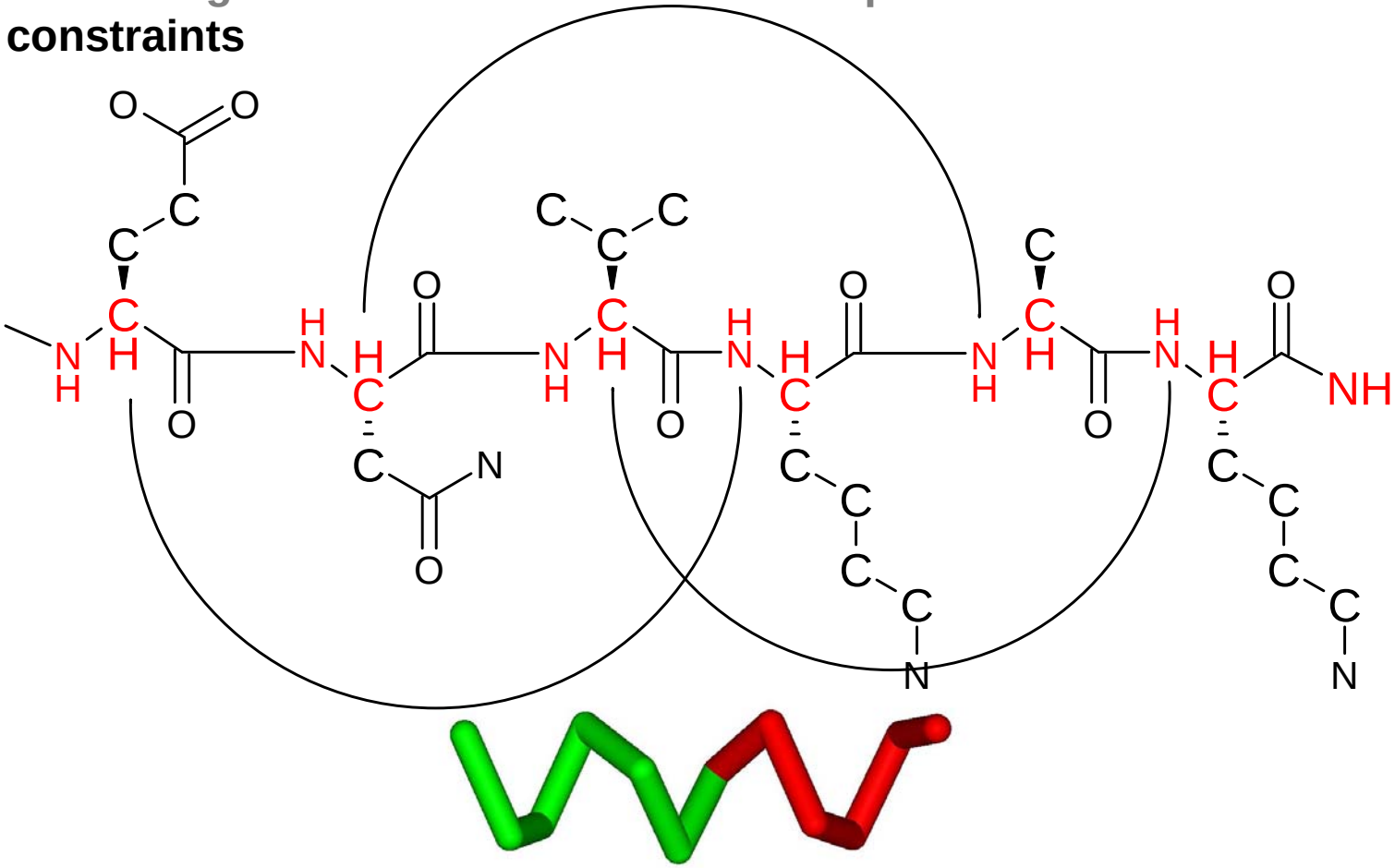

Constraints for structure determination

- Proton-proton distances < 5Å
- Dihedral angle constraints
  - chemical shifts (TALOS+ and TARA)
  - scalar coupling constants
  - stereospecific assignments
- Residual dipolar couplings
  - global relative orientation of bond vectors
  - requires alignment in magnetic field
    - Phage, bicells, stretched gels, etc.
- Hydrogen bond constraints
  - Deduced
  - Cross H-bond scalar coupling

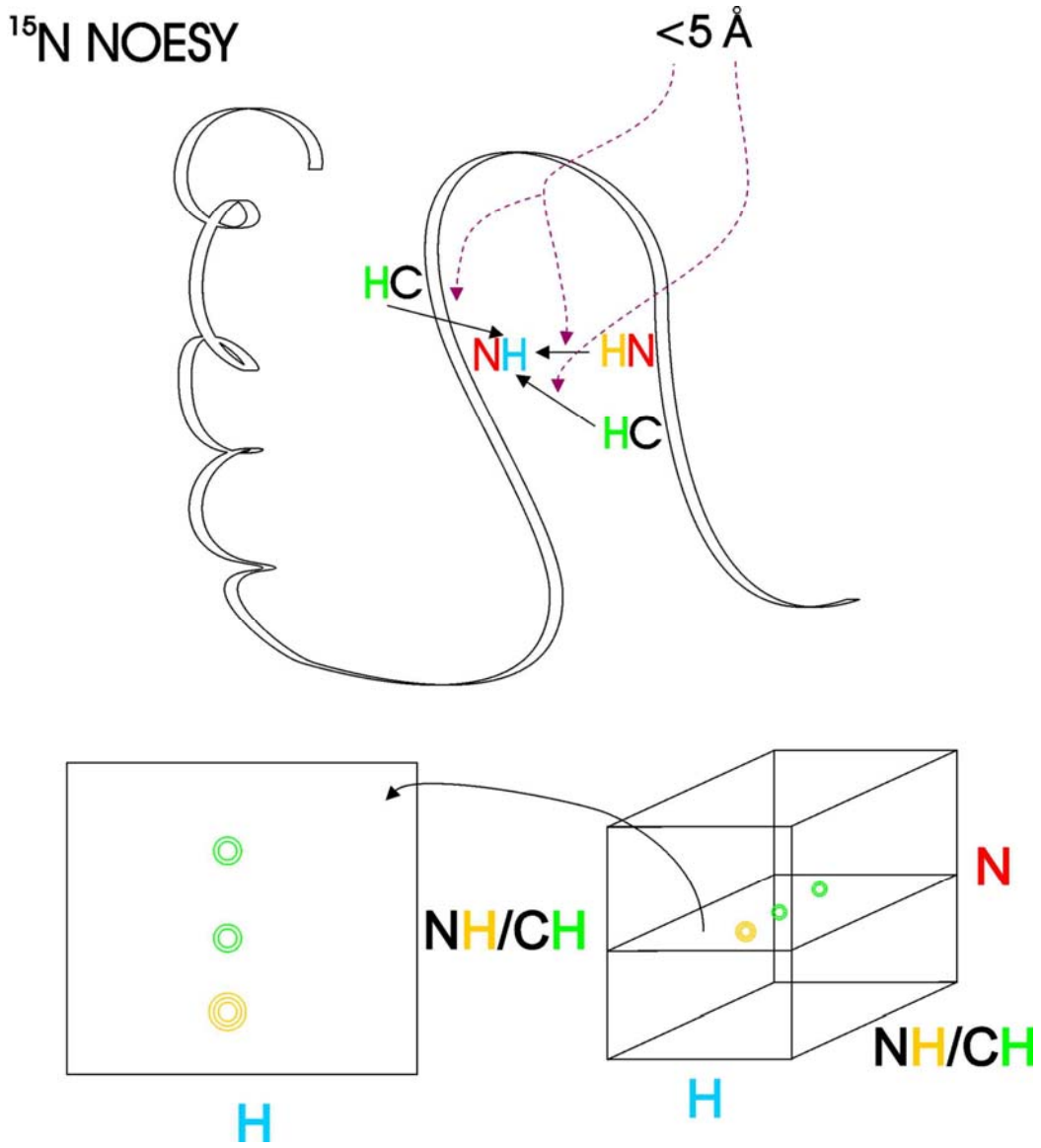
15N NOESY
<5 Å
HC
NH
HN
HC
NH/CH
N
NH/CH
H
H

Random starting structure with predicted secondary structure (from ^{13}C chemical shifts)

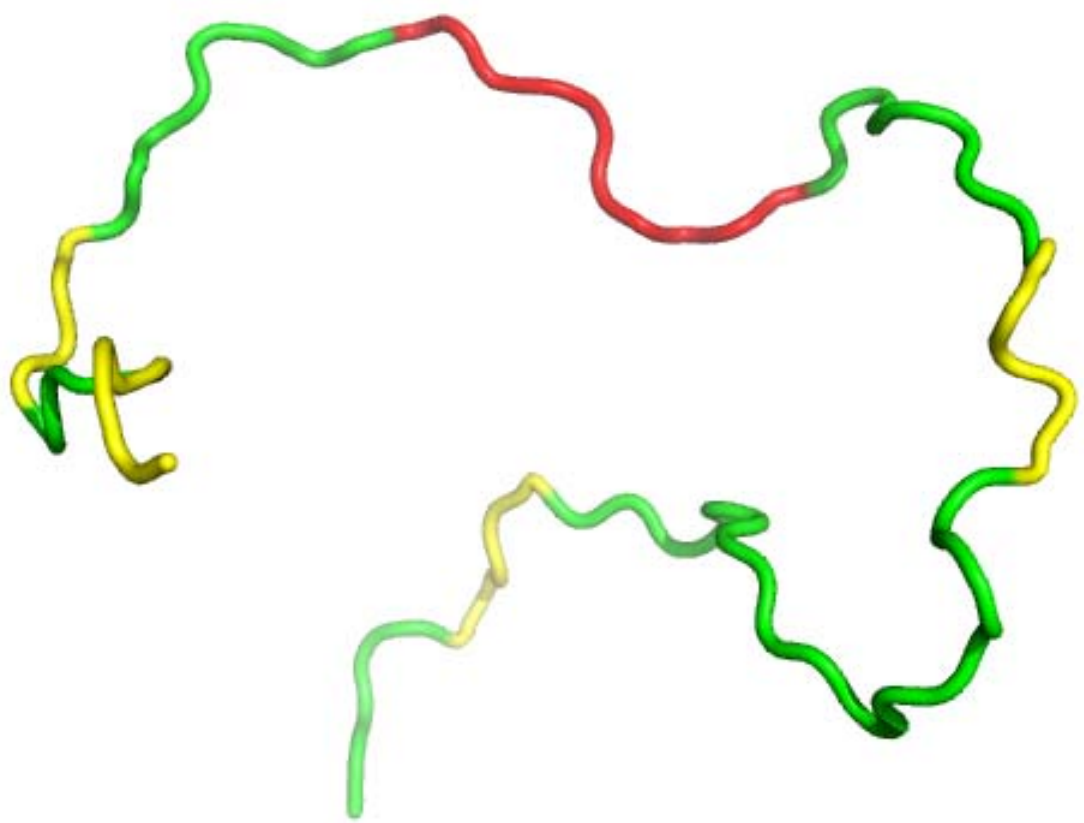

Red: helix
Yellow: sheet
Green: coil

Random structure + all experimental restraints (distances <5Å & dihedral angles)

Folded structure -network of distance restraints

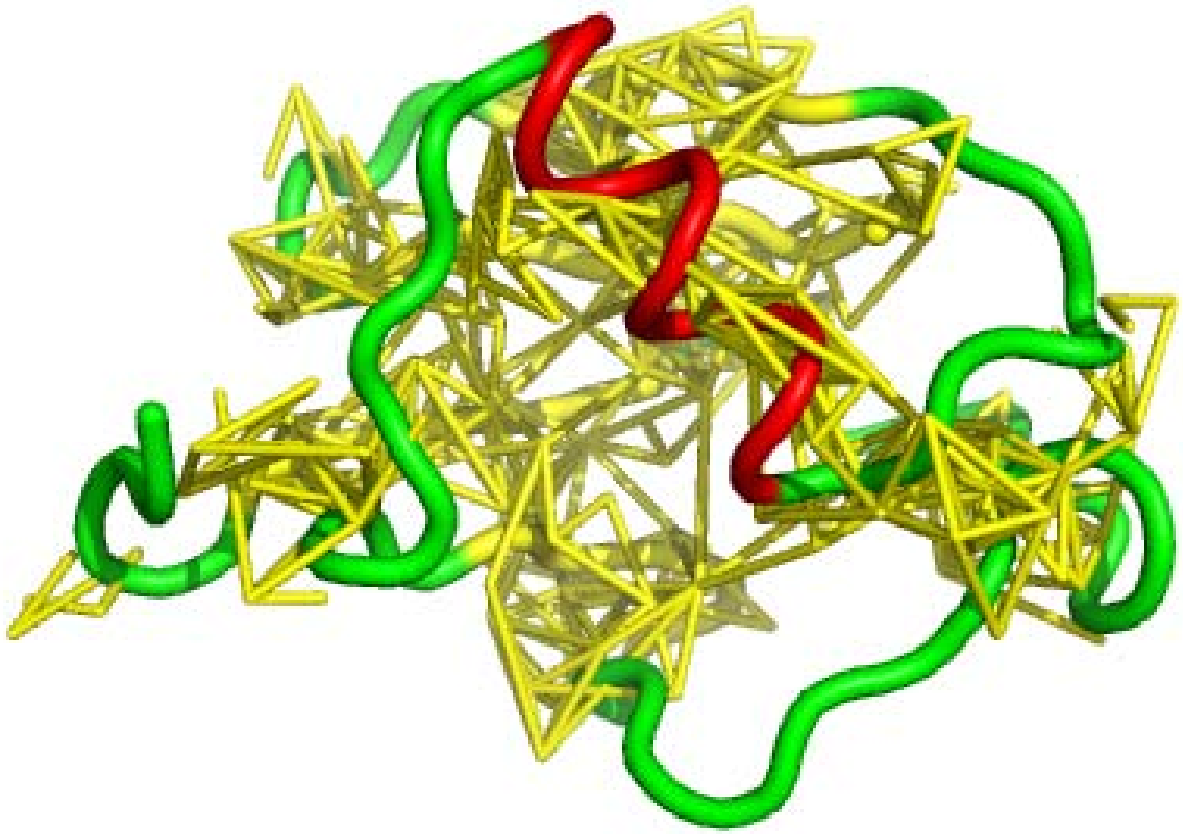

Fourier transform: A linear transform

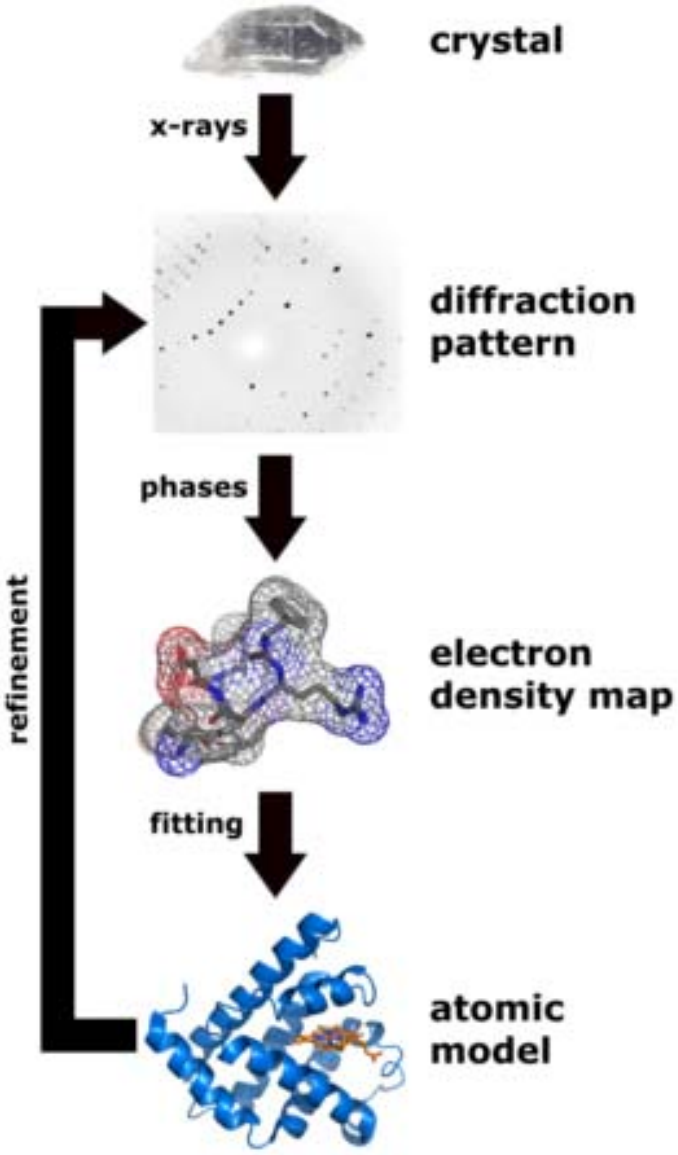

Raw data

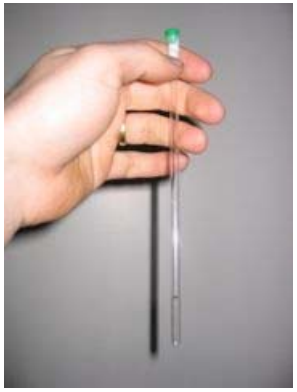

FT

Linear

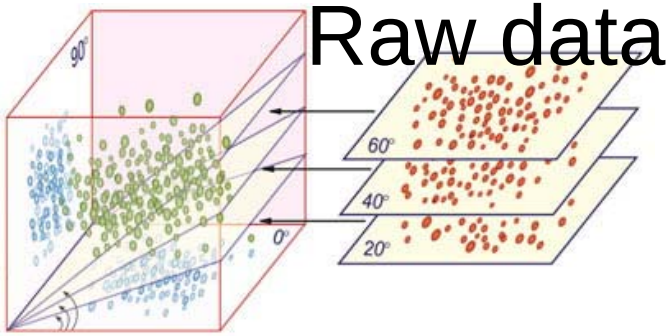

Raw data

- **??-practical solution-??**
  CS-ROSETTA (small proteins)
- **In principle QM (age of universe computation)**

NP-Hard*

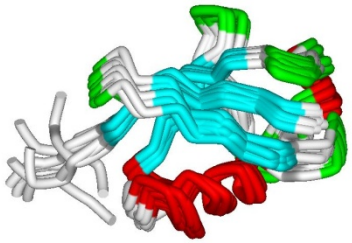

Relaxation matrix analysis

Non-linear

NOE constraints

Assignments

*http://en.wikipedia.org/wiki/P_versus_NP_problem

FT

Linear

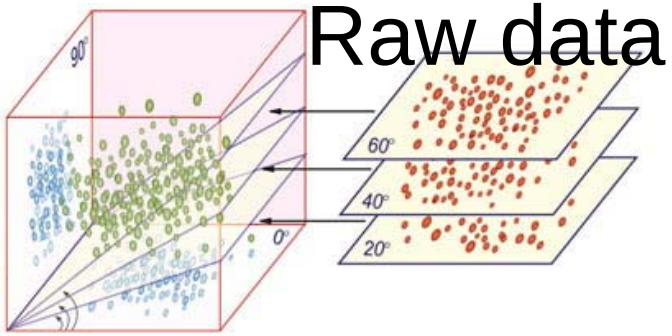

Raw data

- **??-practical solution-??**
  CS-ROSETTA (small proteins)
- **In principle QM (age of universe computation)**

NP-Hard*

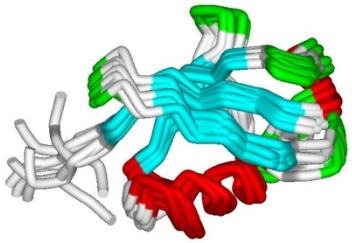

Relaxation matrix analysis

Non-linear

NOE constraints

Assignments

dynamics **binding** **chemistry**

*http://en.wikipedia.org/wiki/P_versus_NP_problem

Vitamin D receptor- Ligand binding domain

Chemical shift perturbations observed in solution by NMR (hormone vs 2MD)

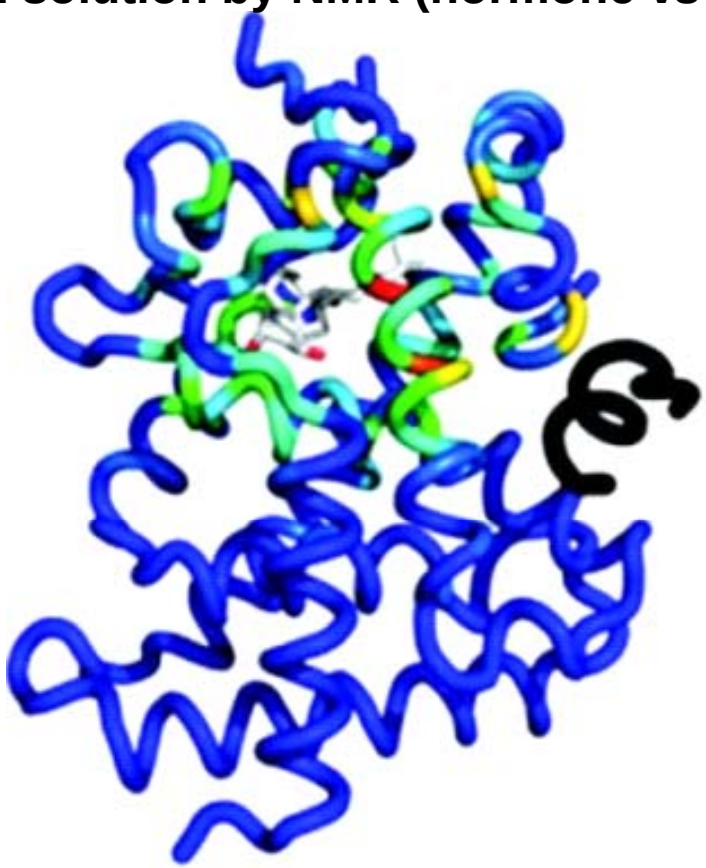

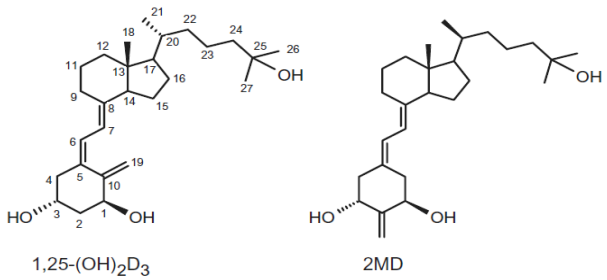

Overlay of 6 crystal structures with different ligands

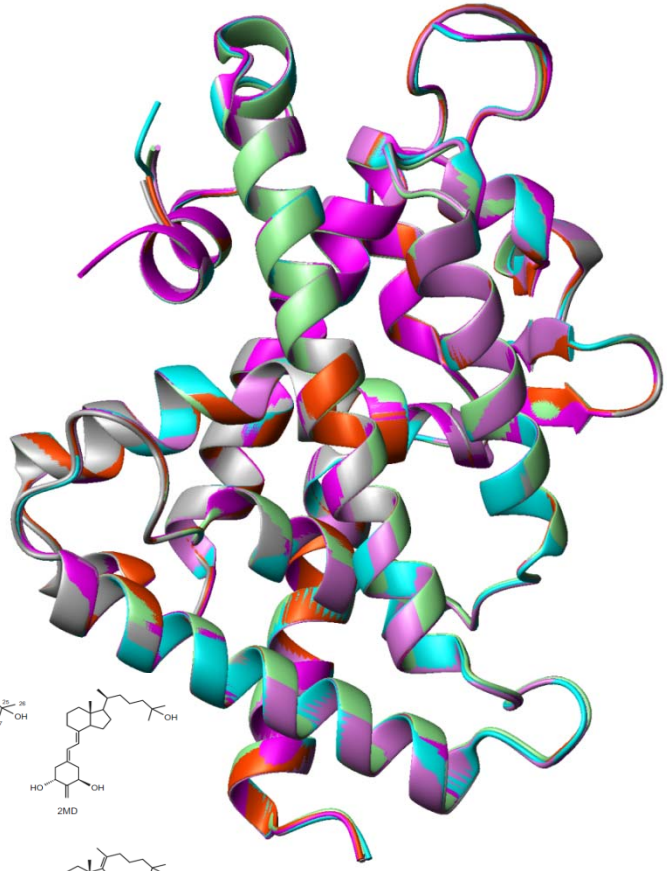

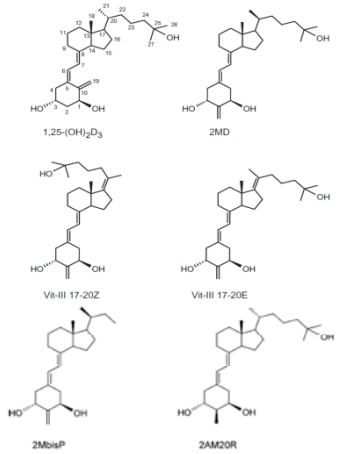

1. Singarapu, K. K. et al. Ligand-Specific Structural Changes in the Vitamin D Receptor in Solution. Biochem. 50, 11025–11033 (2011).

Vitamin D receptor – ligand binding domain

NMR spectral differences observed for 2 different ligands

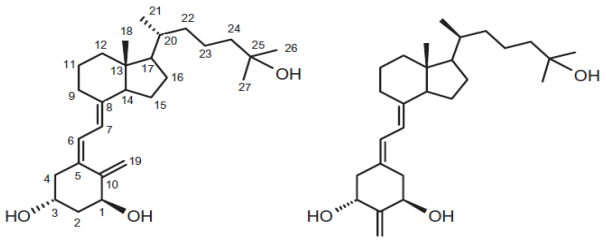

1,25-$(OH)_2D_3$ 2MD

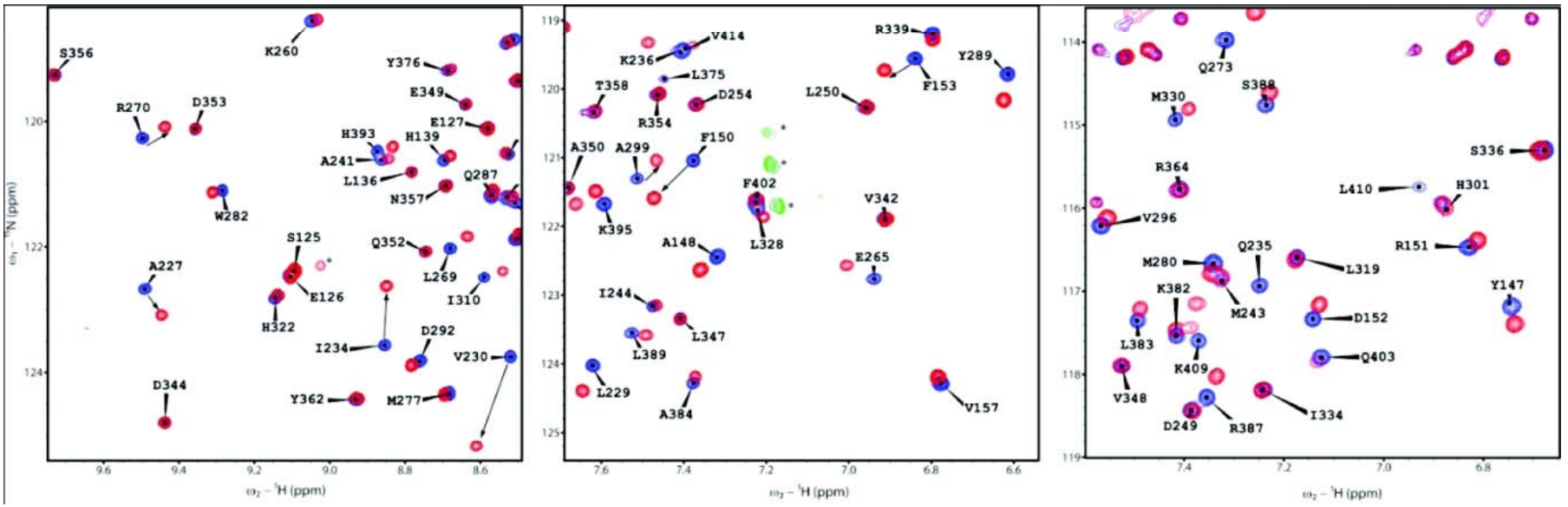

Binding equilibria

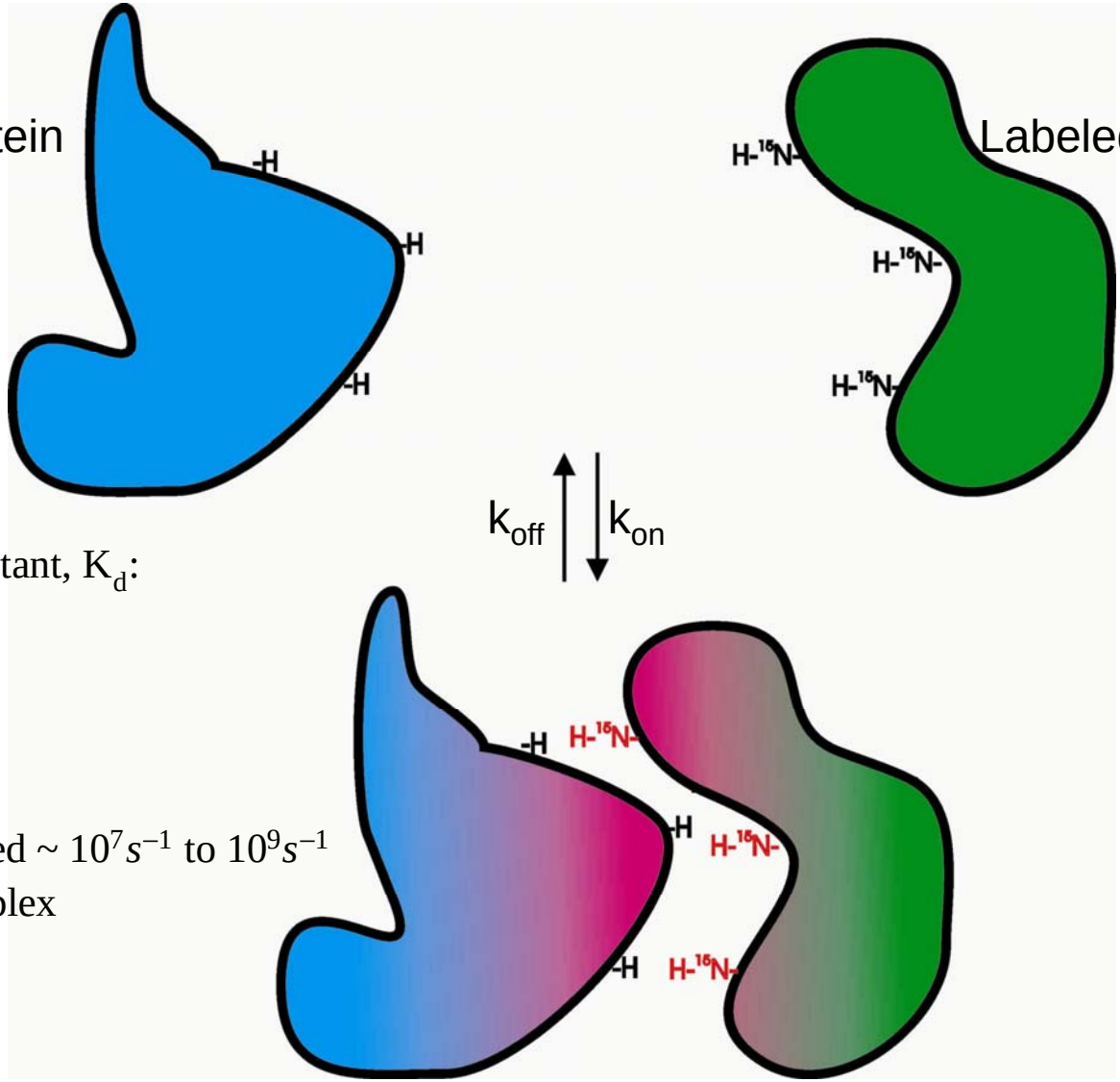

Dissociation equilibrium constant, K_d:

$$AB \underset{k_{on}}{\overset{k_{off}}{\rightleftharpoons}} A + B$$

$$K_d = \frac{k_{off}}{k_{on}} = \frac{[A][B]}{[AB]}$$

k_{on}: usually diffusion controlled ~ $10^7 s^{-1}$ to $10^9 s^{-1}$

k_{off}: characteristic of the complex

$k_{ex} = k_{on} + k_{off}$: exchange rate

Binding curves

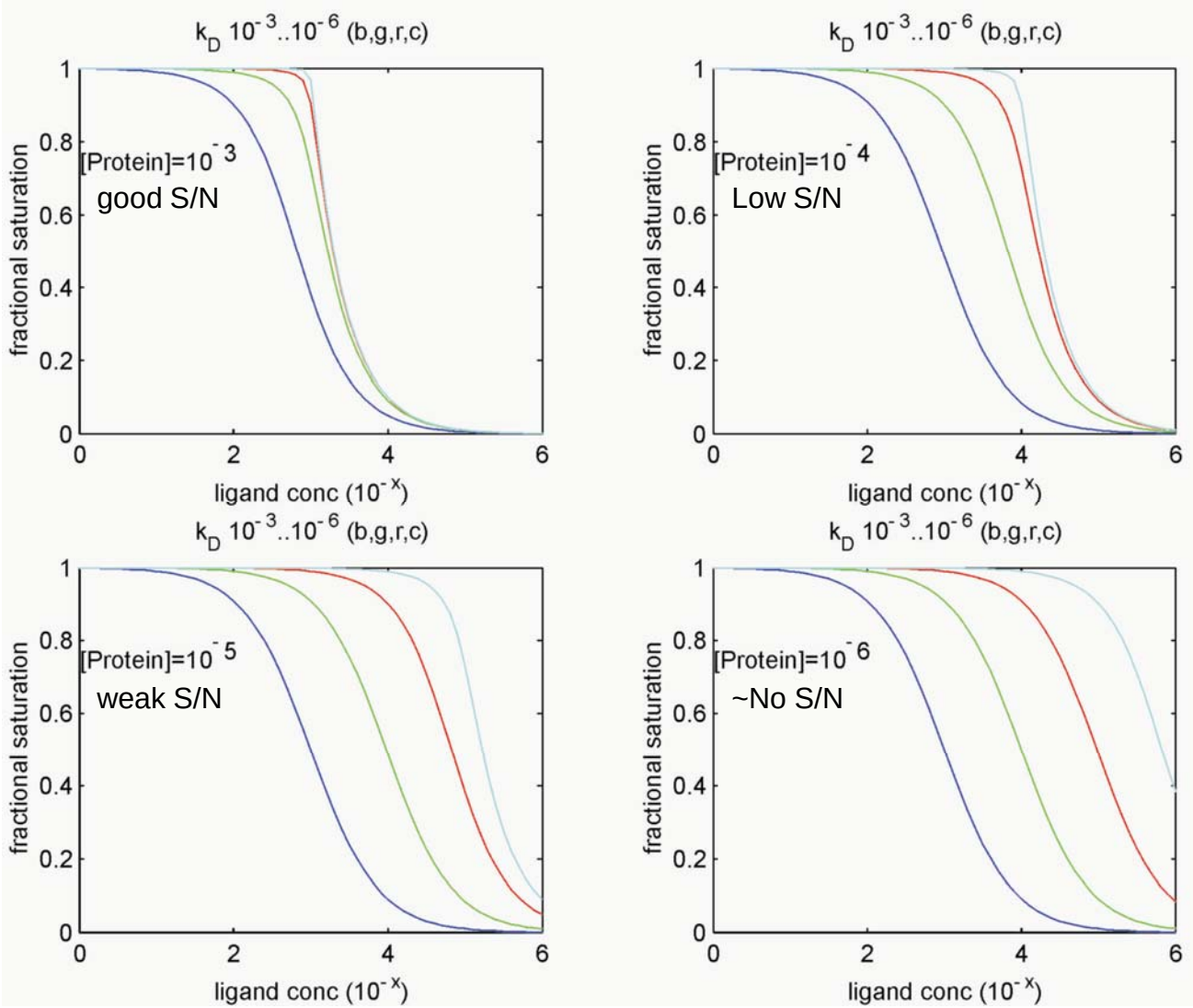

NMR is esp. useful for K_d >10^{-6} (K_d <10^{-6} ok for bound state) and protein concentrations ~50μM-1mM

Chemical shift and line width effects due to exchange (e.g. binding)

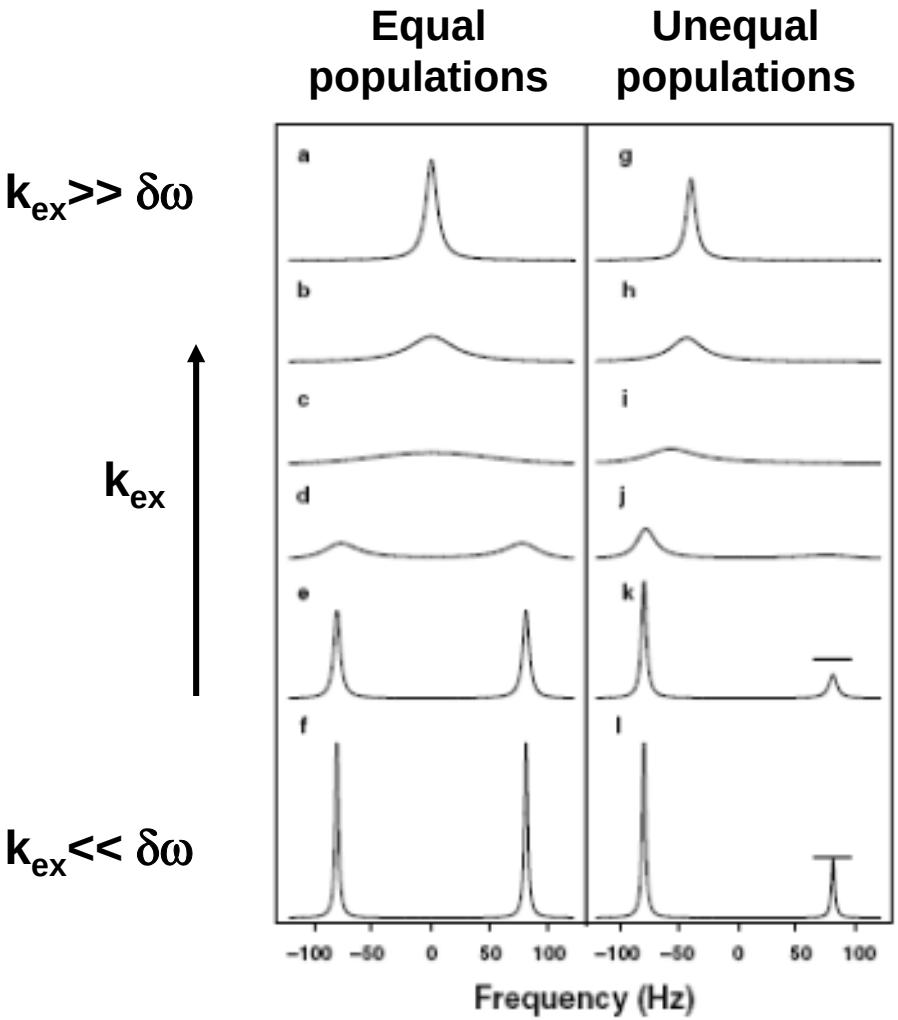

Fast exchange
(averaged line position)
δ=pA*δA+pB*δB

Slow exchange
(two lines)
δA,δB

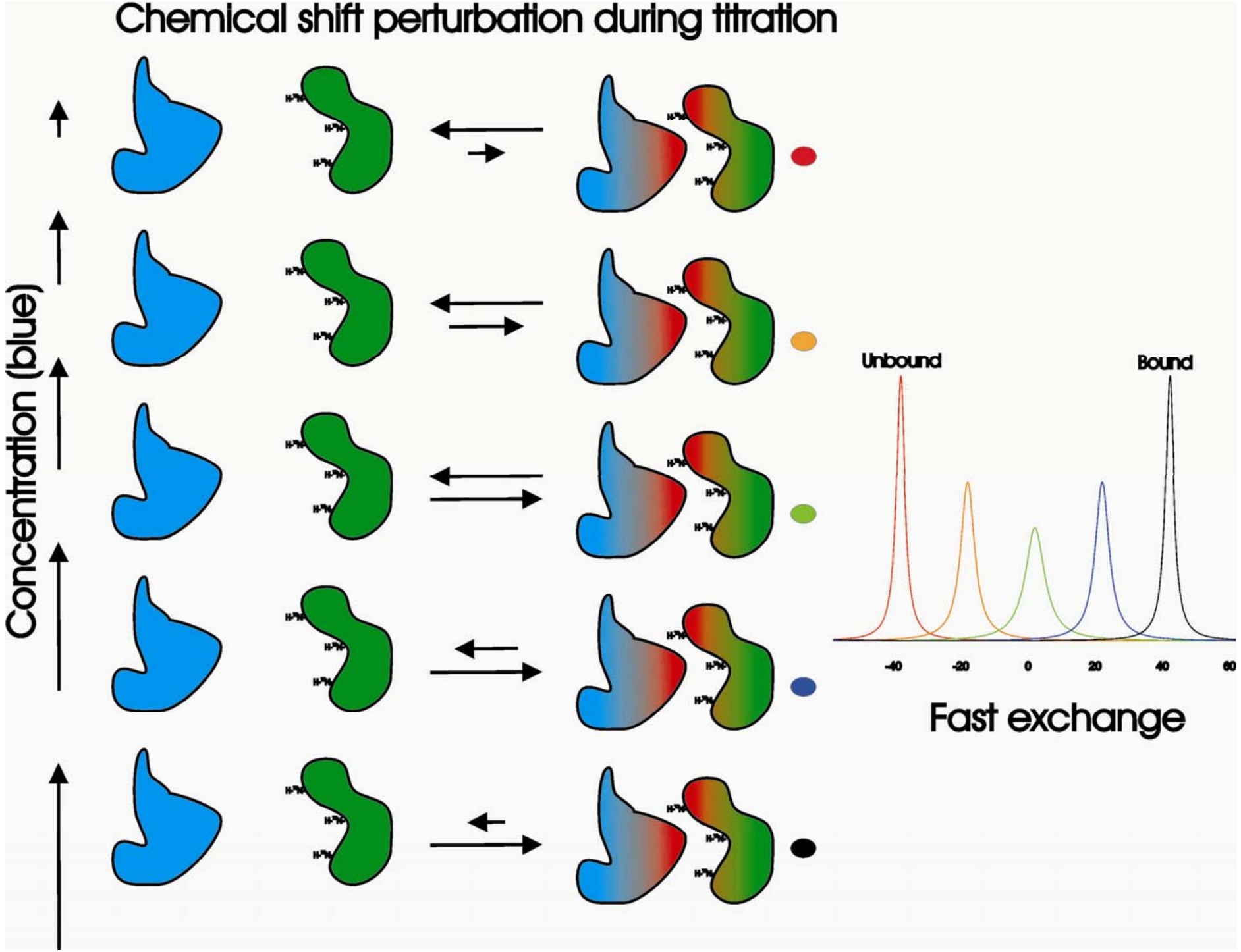
Chemical shift perturbation during titration
Concentration (blue)
Unbound
Bound
-40
-20
0
20
40
60
Fast exchange

Example of ^{1}H-^{15}N HSQC Chemical Shift Titration Under Conditions of Fast Exchange

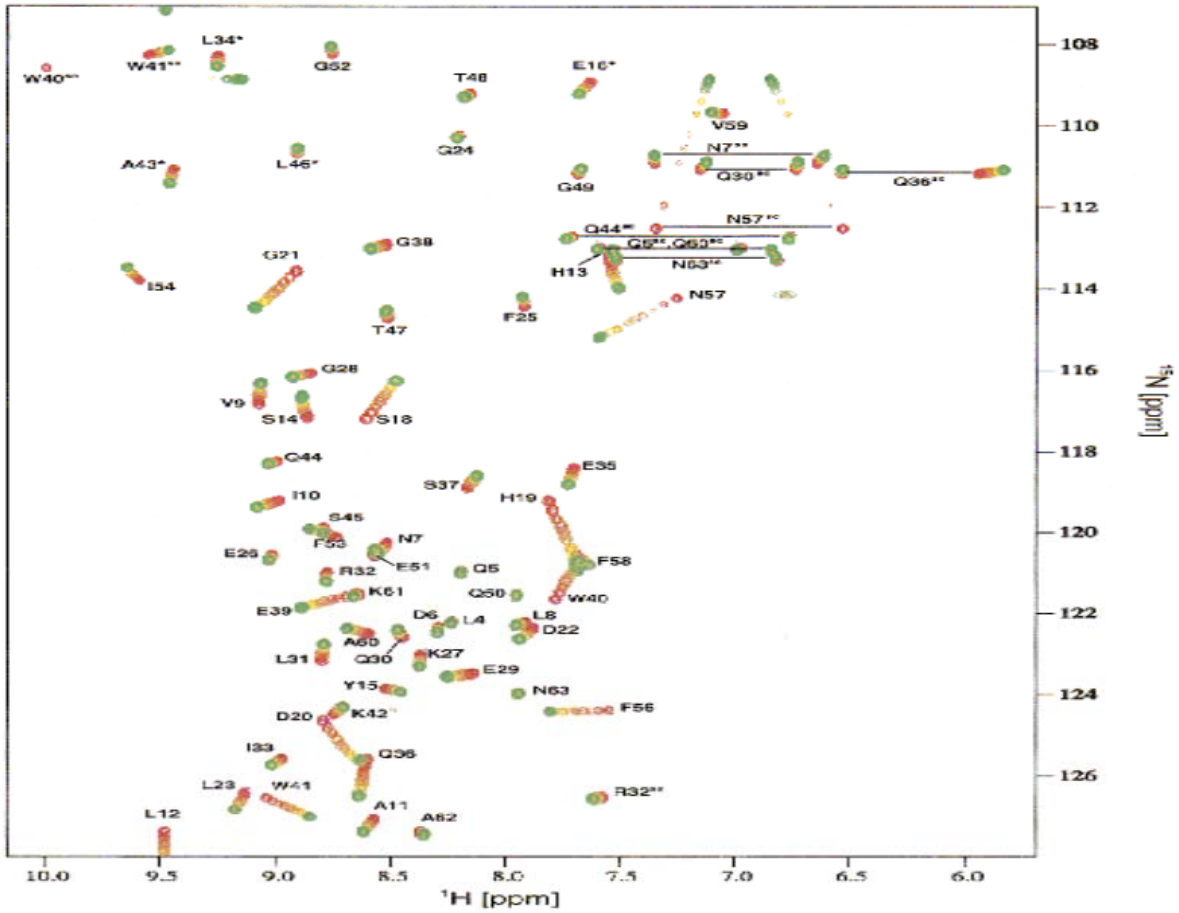

NMR titration experiment showing the changes in the ^{1}H-^{15}N HSQC spectrum of free LckSH3 (red) upon gradual addition of Tip(173-185). Resonances belonging to the spectra after the final step of the titration (4-fold molar excess of Tip) are shown in green.

NOTE that some xpks show signs of intermediate exchange during the titration!

Hydrogen exchange

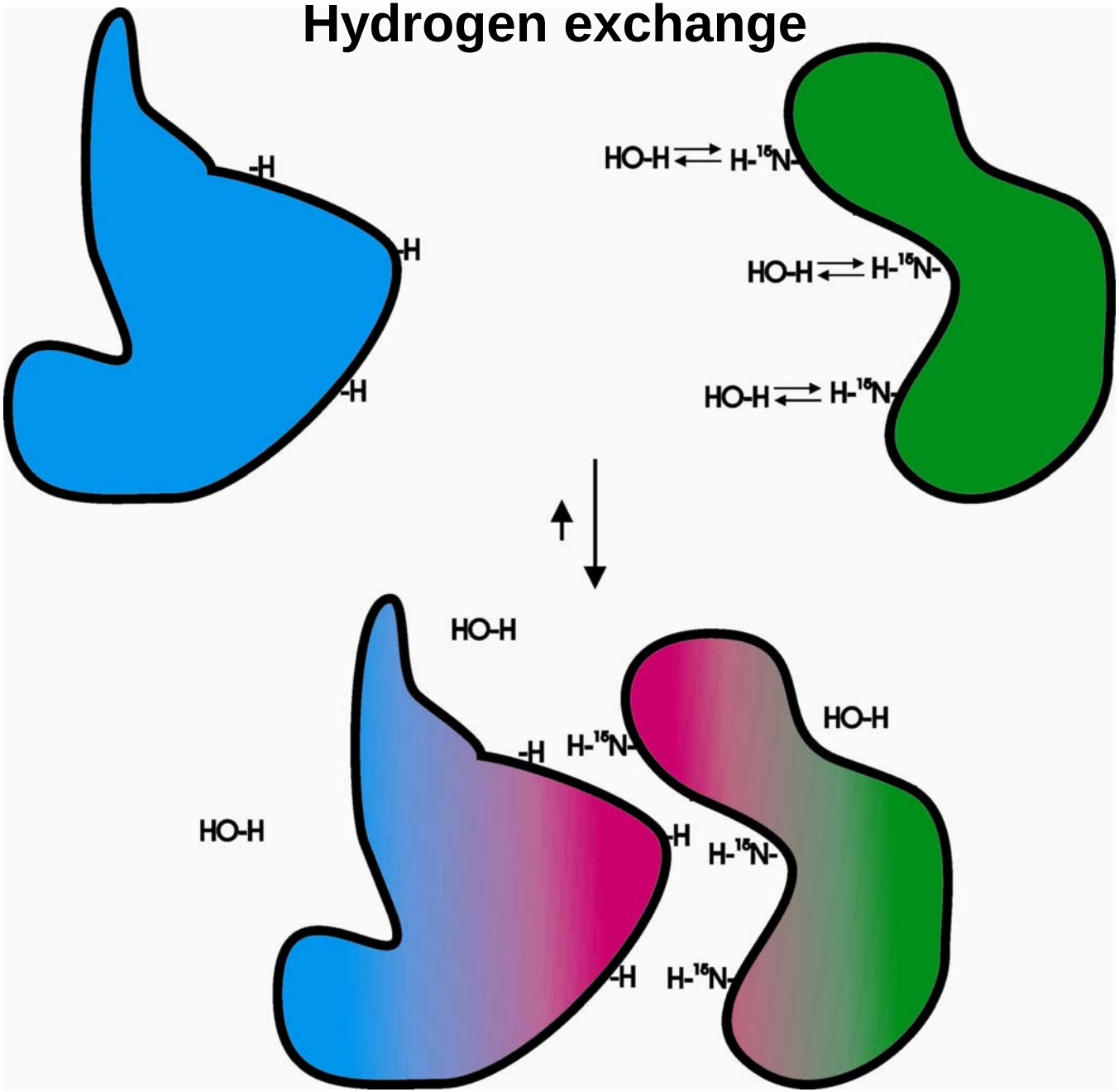

Hydrogen exchange

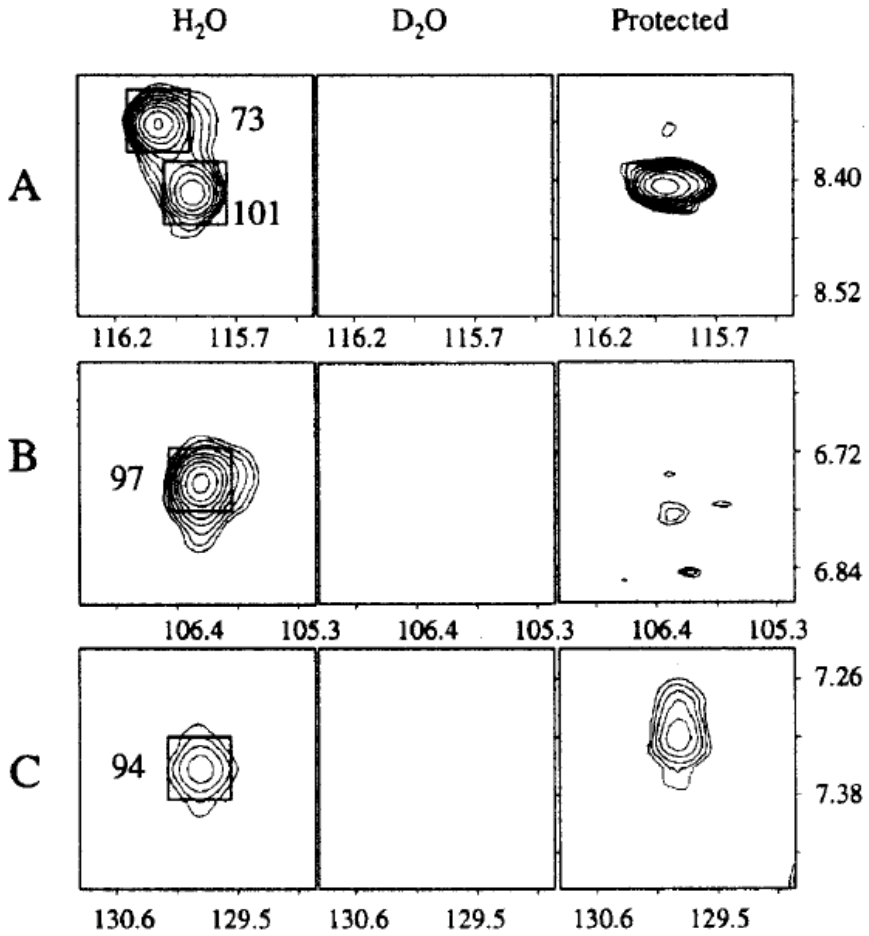

FIG. 2. **Representative exchange data for mAb 7A1.** Portions of the HSQC spectra of Der p 2 containing resonances from residues 73, 101 (*panel A*), 97 (*panel B*), and 94 (*panel C*) are shown. The *left column* of spectra were obtained for a sample in H_2O. The *middle column* of spectra were obtained from a sample of Der p 2 in D_2O. The *right column* (*Protected*) of spectra were obtained from a sample that was bound to mAb 7A1 for 48 h in the presence of D_2O.

Mueller, G. , Smith, M., Chapman, M. D., Rule, G. S. & Benjamin, D. C. Hydrogen exchange nuclear magnetic resonance spectroscopy mapping of antibody epitopes on the house dust mite allergen Der p 2. The Journal of biological chemistry 276, 9359–65 (2001).

Hydrogen exchange

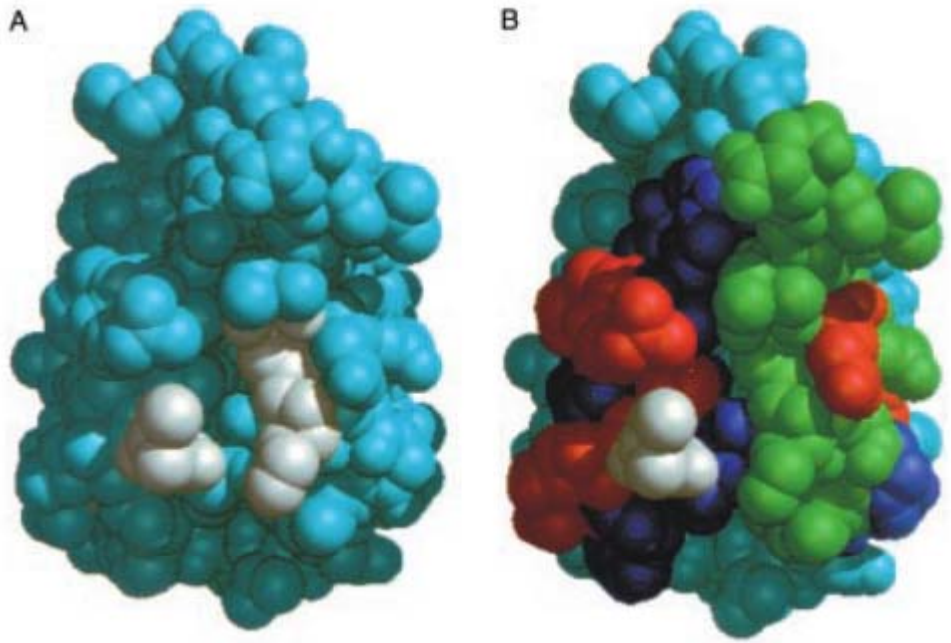

FIG. 4. **Functionally important residues in the 7A1 epitope.** *A*, space-filling model showing the residues (*white*) protected by the 7A1 mAb during the NMR amide-proton protection assay. *B*, the residues important for mAb 7A1 binding are mapped onto a surface representation of Der p 2. The view is looking down the end of the β-barrel where mAb 7A1 is proposed to interact. The color scheme is as follows: *red*, residues that when mutated to alanine significantly affect the binding of Der p 2 to mAb 7A1. *White*, Lys-97, which was the only residue protected in the amide-protection assay, which, when mutated, significantly affected binding. *Green*, residues that when mutated to alanine did not affect antibody binding. *Blue*, residues that were not mutated.

Cross-saturation

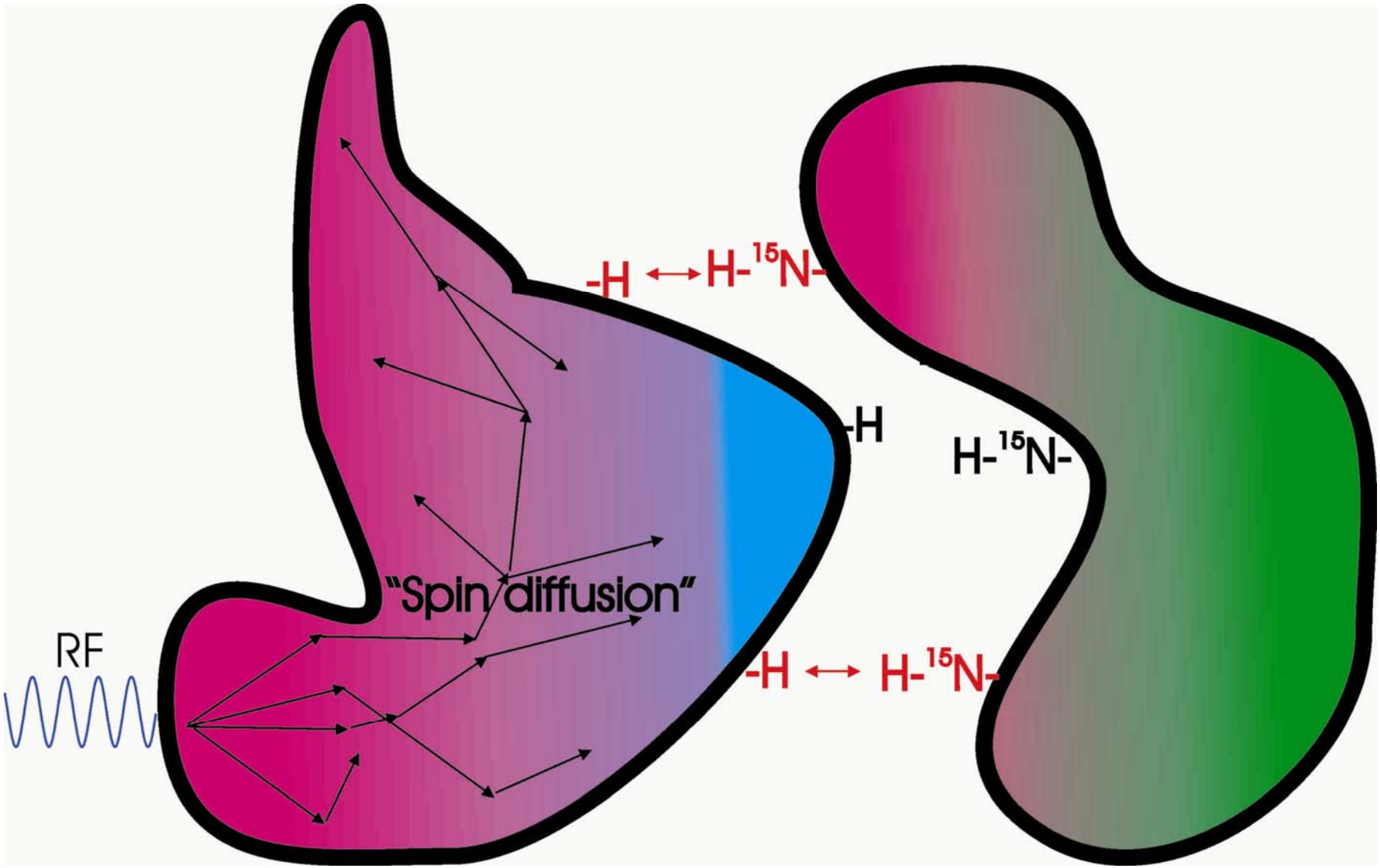

Cross-saturation

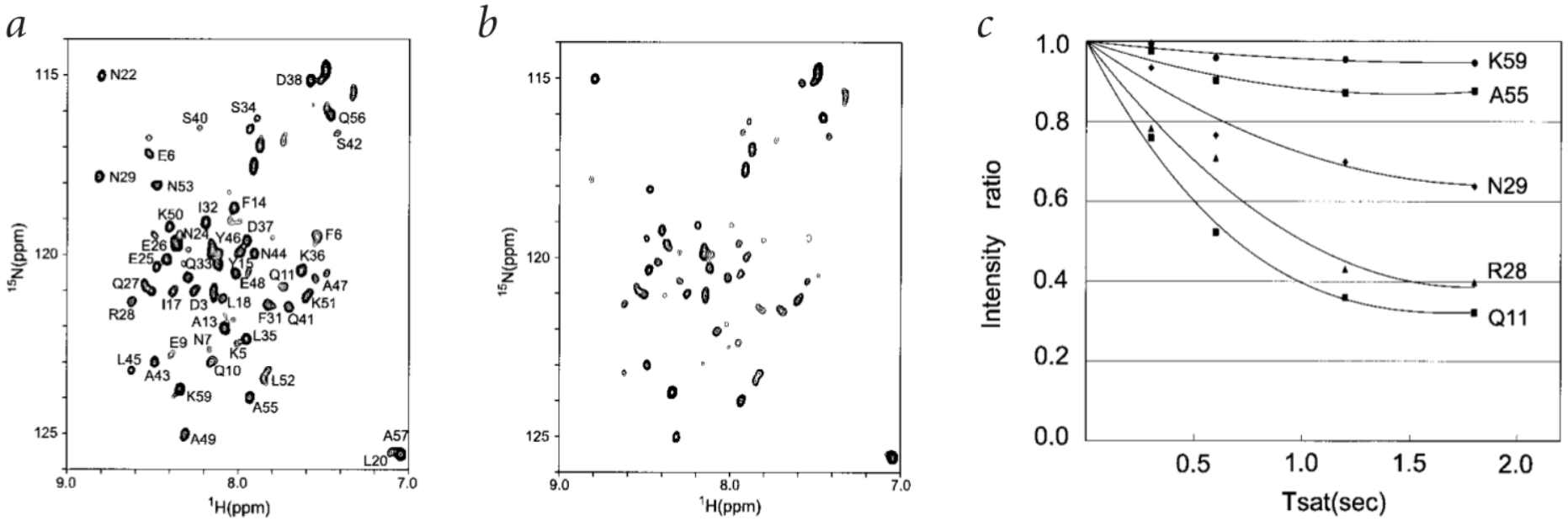

Fig. 3 The results of the cross-saturation experiment. ^{1}H-^{15}N TROSY-HSQC spectra observed for uniformly ^{2}H,^{15}N-labeled FB in complex with the Fc fragment in 10% H_2O/90% $^{2}H_2O$, ***a***, without and ***b***, with irradiation. The spectra were measured with a reasonable protein concentration (0.5–1.0 mM) and within a reasonable measurement time (20 h). ***c***, Effect of the saturation time on the intensity ratios of the crosspeaks originating from the backbone amide groups with irradiation to those without irradiation. The saturation times used were 0.3, 0.6, 1.2 and 1.8 s.

Takahashi, H., Nakanishi, T., Kami, K., Arata, Y. & Shimada, I. A novel NMR method for determining the interfaces of large protein-protein complexes. Nature structural biology 7, 220–3 (2000).

Cross-saturation

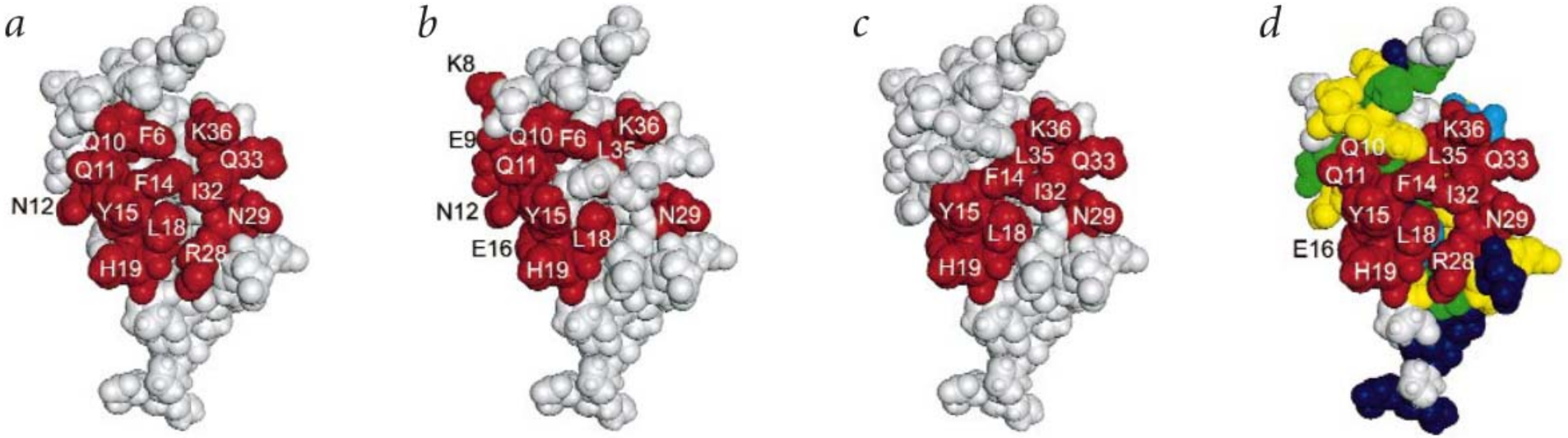

Fig. 5 Comparison of the binding sites of the FB–Fc complex. ***a***, The X-ray crystallography study, ***b***, the chemical shift perturbation, ***c***, the H-D exchange experiments, and ***d***, the cross-saturation experiment. Residues with accessible surface areas that are covered upon binding of the Fc fragment (Phe 6, Gln 10, Gln 11, Asn 12, Phe 14, Tyr 15, Leu 18, His 19, Arg 28, Asn 29, Ile 32, Gln 33 and Lys 36)[9] are colored in red in (*a*). Residues showing absolute values of chemical shift difference ($[(\Delta H_N)^2 + (\Delta N \times 0.15)^2]^{1/2}$) of more than 0.2 p.p.m. (Phe 6, Lys 8, Glu 9, Gln 10, Gln 11, Asn 12, Ala 13, Tyr 15, Glu 16, Leu 18, His 19, Asn 29, Gly 30, Leu 35, Lys 36 and Ser 40) are colored in red in (*b*). Out of these residues, Ala 13, Gly 30 and Ser 40 are buried in the molecule. On the basis of the BioMagResBank database at http://www.bmrb.wisc.edu, the scale factor of 0.15 used for normalization of the magnitude of ^{15}N chemical shift changes (in p.p.m. units) was derived from the average (over all residue types but proline) standard deviations for the backbone ^{1}HN and ^{15}N chemical shifts. Residues showing protection factors of larger than 10 upon binding of the Fc fragment (Phe 14, Tyr 15, Glu 16, Ile 17, Leu 18, His 19, Asn 29, Ile 32, Gln 33, Leu 35, Lys 36, Leu 46, Ala 49, and Lys 50) are colored in red in (*c*)[5]. Out of these residues, Glu 16, Ile 17, Leu 46, Ala 49, and Lys 50 are buried in the molecule. Residues with intensity ratios less than 0.5 (Gln 10, Gln 11, Phe 14, Tyr 15, Glu 16, Leu 18, His 19, Arg 28, Asn 29, Ile 32, Gln 33, Leu 35 and Lys 36), 0.5–0.6, 0.6–0.7, 0.7–0.8 and larger than 0.8 are colored in red, light blue, yellow, green and dark blue, respectively in (*d*). Molecular graphics images were produced using MidasPlus (University of California, San Francisco)[20,21].

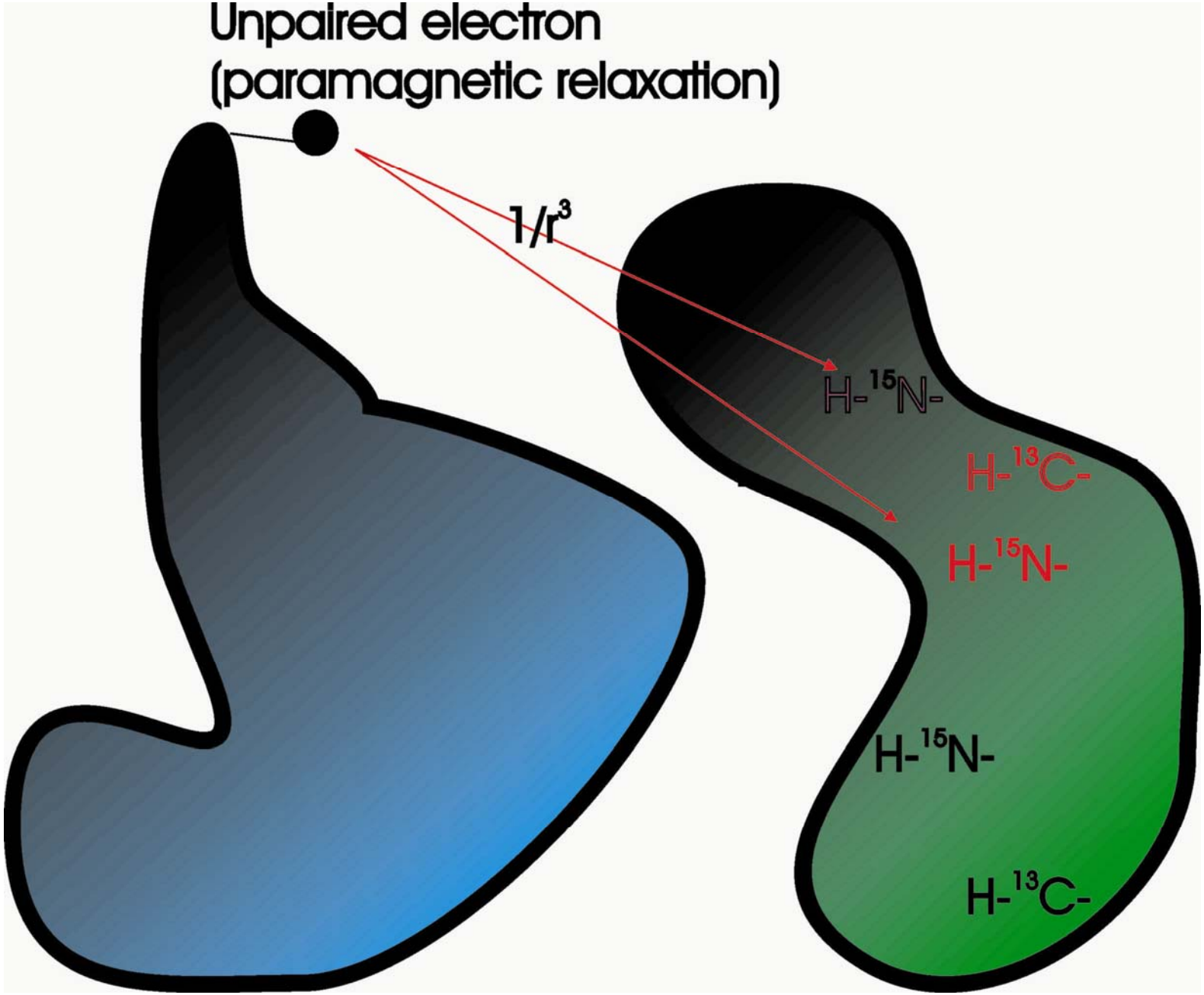
Unpaired electron
(paramagnetic relaxation)
1/r3
H-15N-
H-13C-
H-15N-
H-15N-
H-13C-

PRE- Paramagnetic relaxation enhancement

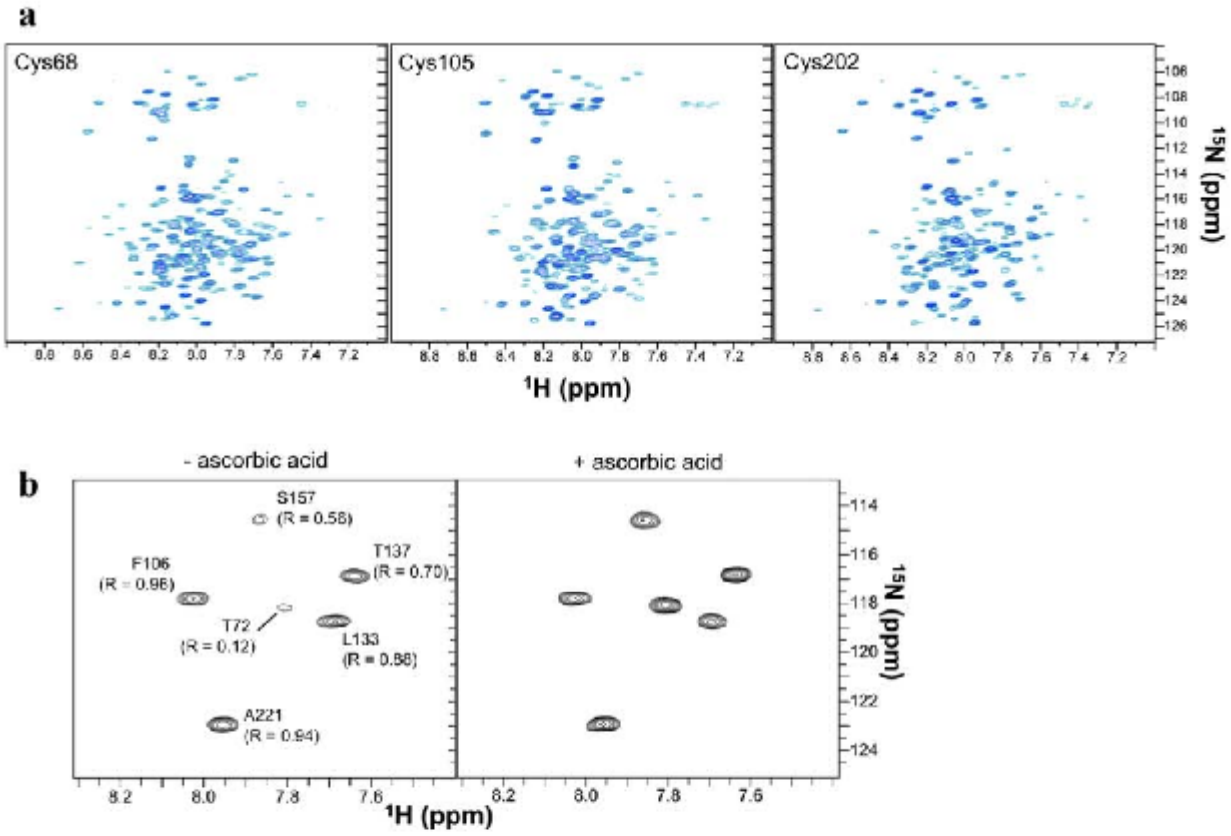

Supplementary Figure 6. PRE measurements in spin-labeled UCP2. **a,** ^{1}H-^{15}N TROSY-HSQC spectra of 3 UCP2 samples with single nitroxide labeled at different cysteine positions. The spectra were recorded after the nitroxide was reduced by the ascorbic acid. **b,** Residue-specific broadening of NMR resonance by a particular spin label (in this case at position 68) was measured with two 3D TROSY-HNCO spectra, one recorded after nitroxide labeling (left) and another after reducing the nitroxide free electron with a 5x molar ascorbic acid (right).

PRE- Paramagnetic relaxation enhancement

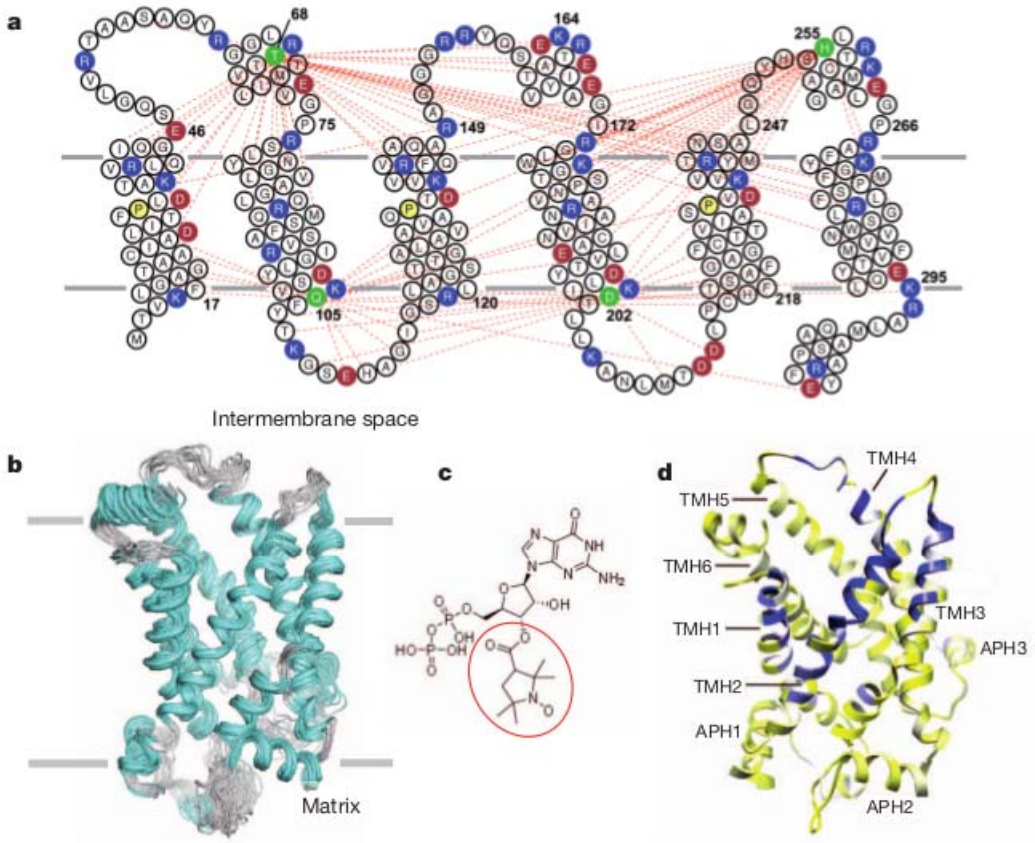

Figure 3 | Solution structure of UCP2 and region of GDP binding. **a**, UCP2 sequence and membrane topology, with basic and acidic residues shown in blue and red, respectively. The conserved prolines at the proline kinks of TMHs 1, 3 and 5 are shown in yellow. The spin-labelled positions are highlighted in green. The red dashed lines represent long-range or interhelical PRE distances (<19 Å) between the spin-label and backbone amide protons. **b**, An ensemble of 15 low-energy structures derived from NMR restraints. The backbone and heavy-atom root mean squared deviations for the structured segments in Fi are 1.2 and 1.8 Å, respectively. **c**, Chemical structure of the spin-labelled GI with the paramagnetic nitroxide moiety circled in red. **d**, Mapping the effec spin-labelled GDP onto the ribbon drawing of UCP2. The colour gradient from yellow (resonance intensity ratio of broadened to non-broadened, ε = to white ($\varepsilon = 0.8$) to blue ($\varepsilon = 0.3$).

Berardi, M. J., Shih, W. M., Harrison, S. C. & Chou, J. J. Mitochondrial uncoupling protein 2 structure determined by NMR molecular fragment searching. Nature 476, 109–13 (2011).

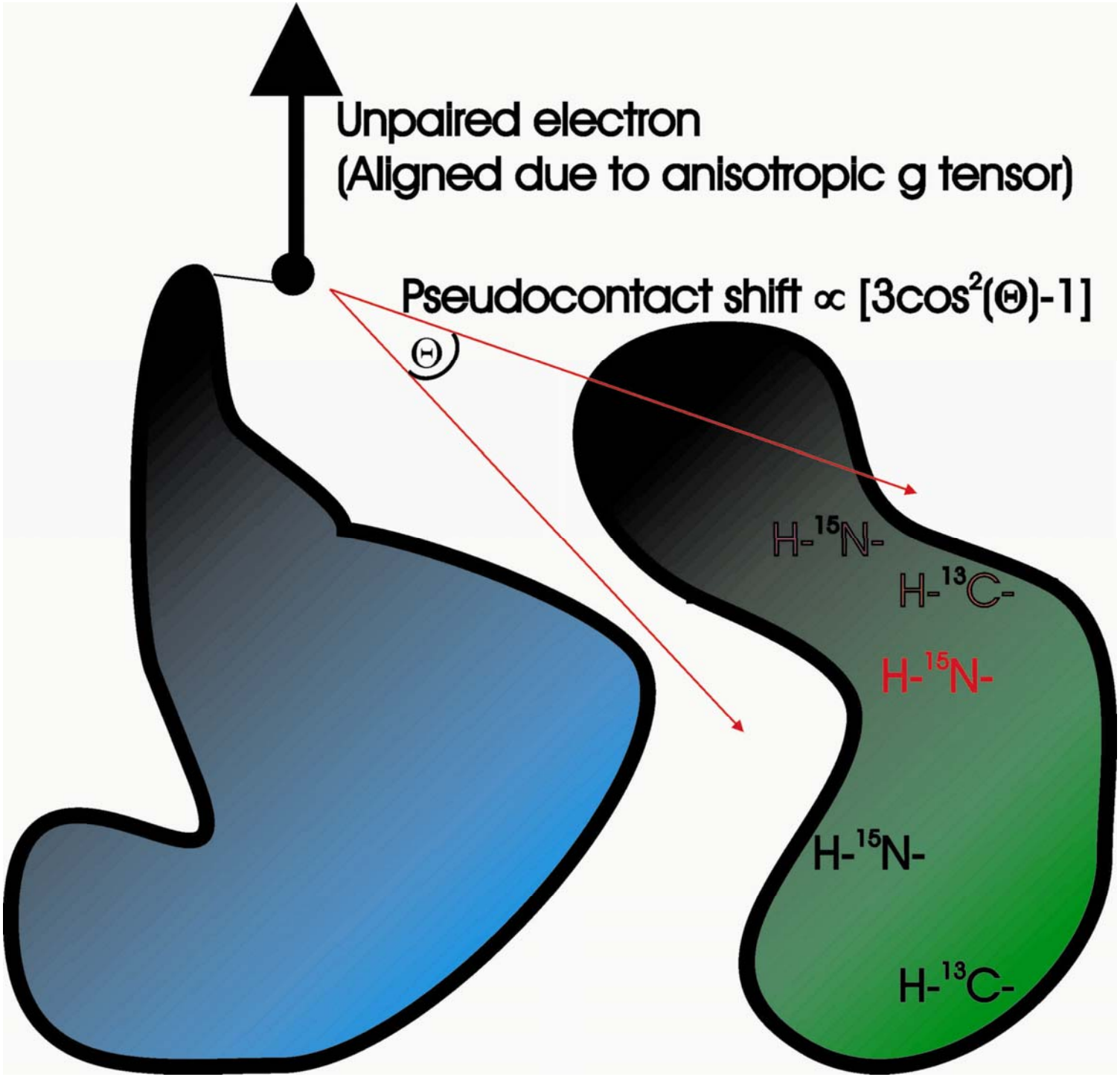
Unpaired electron
(Aligned due to anisotropic g tensor)
Pseudocontact shift ∝ [3cos²(Θ)-1]
Θ
H-15N-
H-13C-
H-15N-
H-15N-
H-13C-

Paramagnetic pseudocontact shift

Figure 2

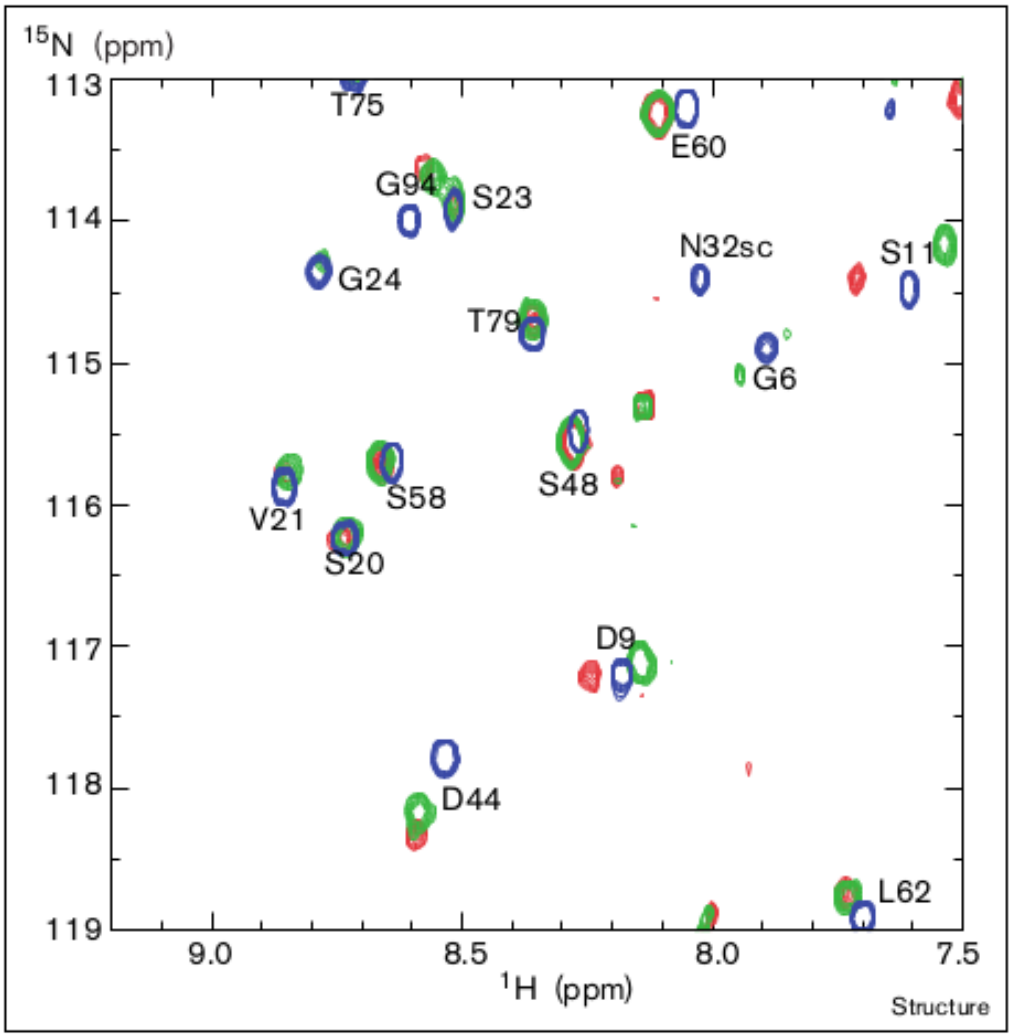

Overlay of part of the ^{15}N-HSQC spectra of free plastocyanin (blue), plastocyanin and reduced cytochrome *f* (green), and plastocyanin and oxidized cytochrome *f* (red). The cytochrome *f*:plastocyanin ratio was 0.8.

Paramagnetic pseudocontact shift

Figure 6

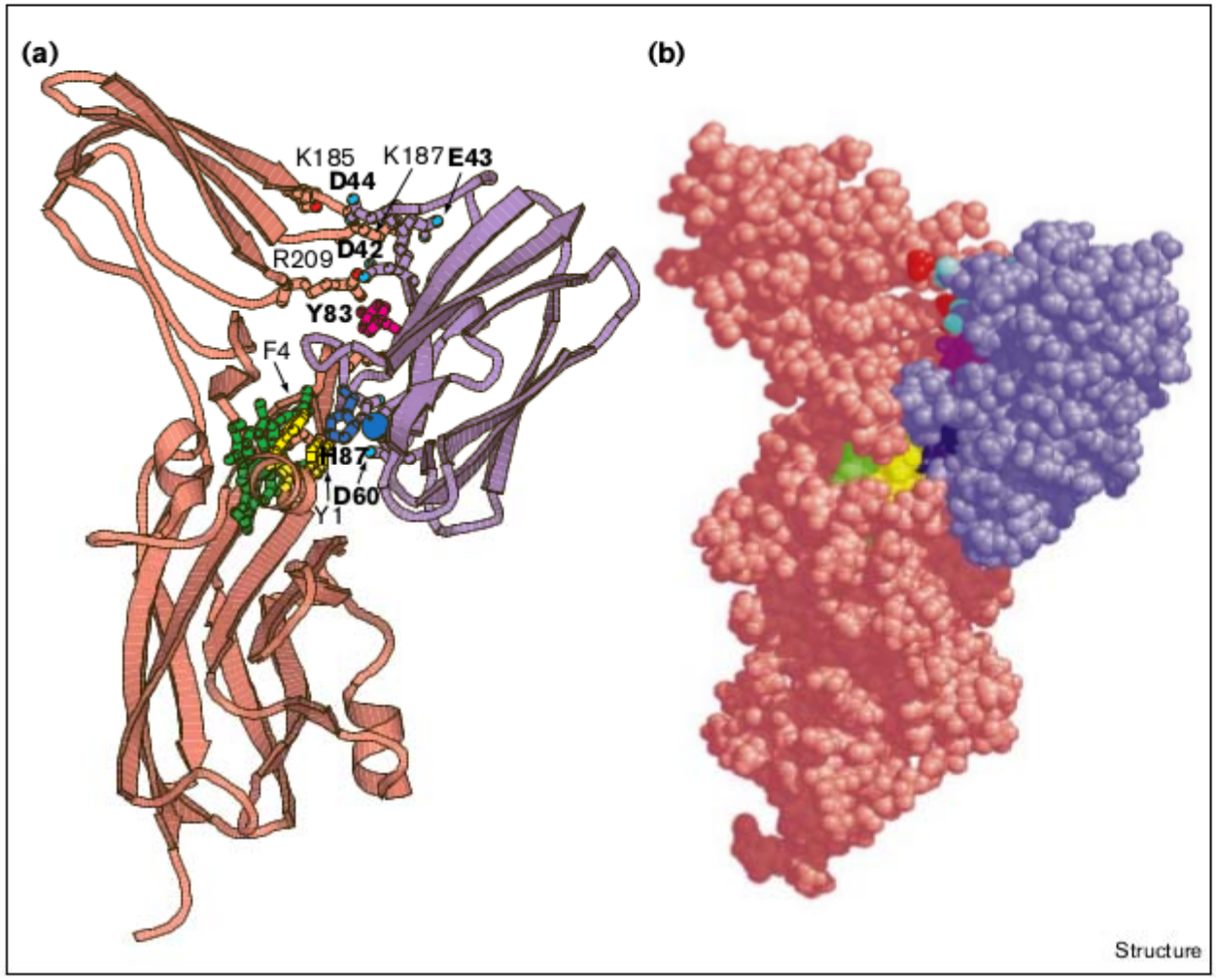

The structure of the plastocyanin–cytochrome *f* complex. The structure of the complex is shown with plastocyanin in purple and cytochrome *f* in orange in **(a)** backbone and **(b)** spacefilling representations, shown in identical orientations. The color coding is green, haem; yellow, Tyr1 and Phe4; red, Nζ and Nη atoms of Lys185, Lys187 and Arg109; dark blue, His87 and copper; magenta, Tyr83; cyan, Oδ/ε atoms of Asp42, Glu43, Asp44 and Asp60. Plastocyanin residues are indicated in bold text.

Ubbink, M., Ejdebäck, M., Karlsson, B. G. & Bendall, D. S. The structure of the complex of plastocyanin and cytochrome f, determined by paramagnetic NMR and restrained rigid-body molecular dynamics. Structure (London, England : 1993) 6, 323–35 (1998).

Residual Dipolar coupling (RDC)
requires alignment media (phage, bicelles,...)

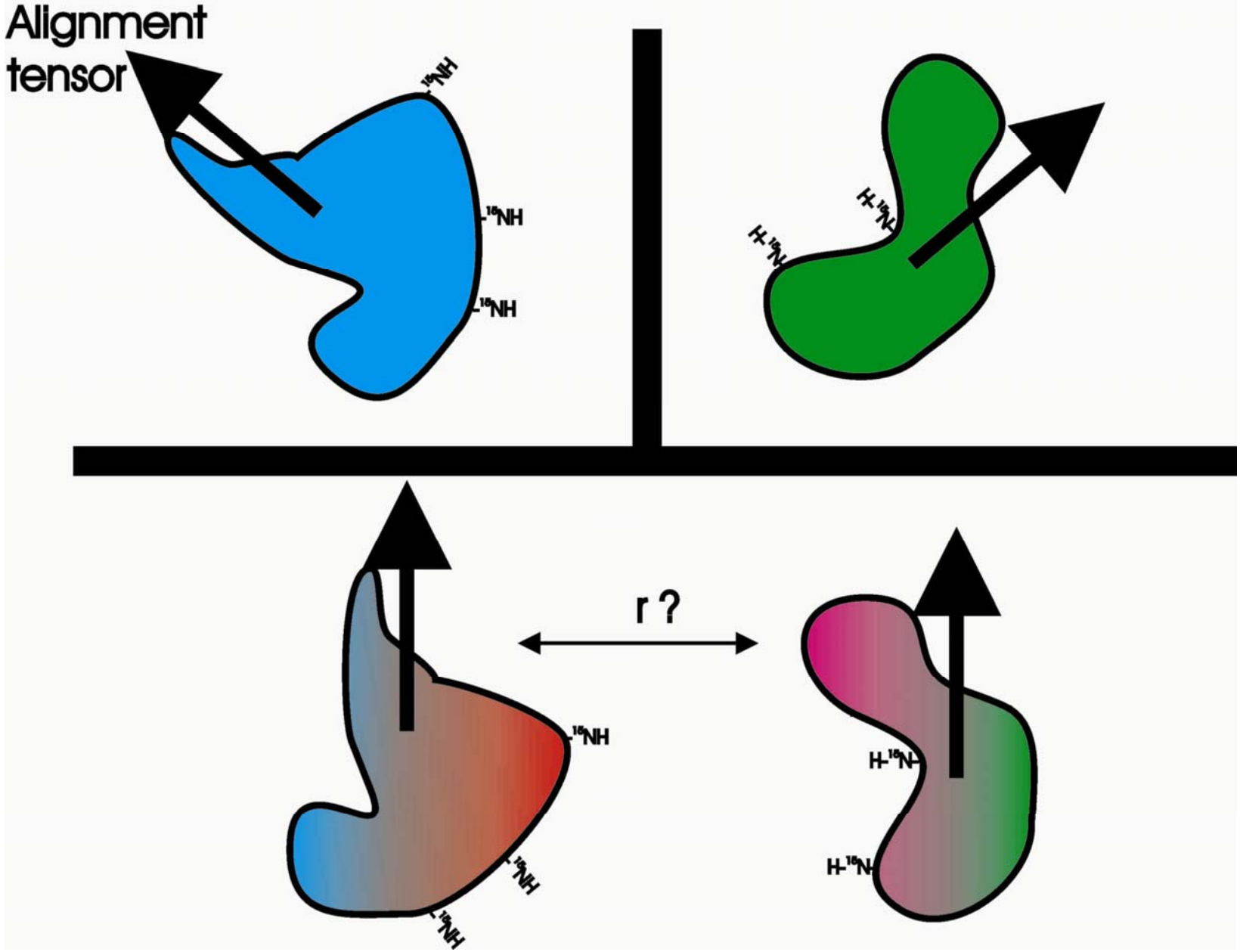

Residual dipolar couplings (RDC)

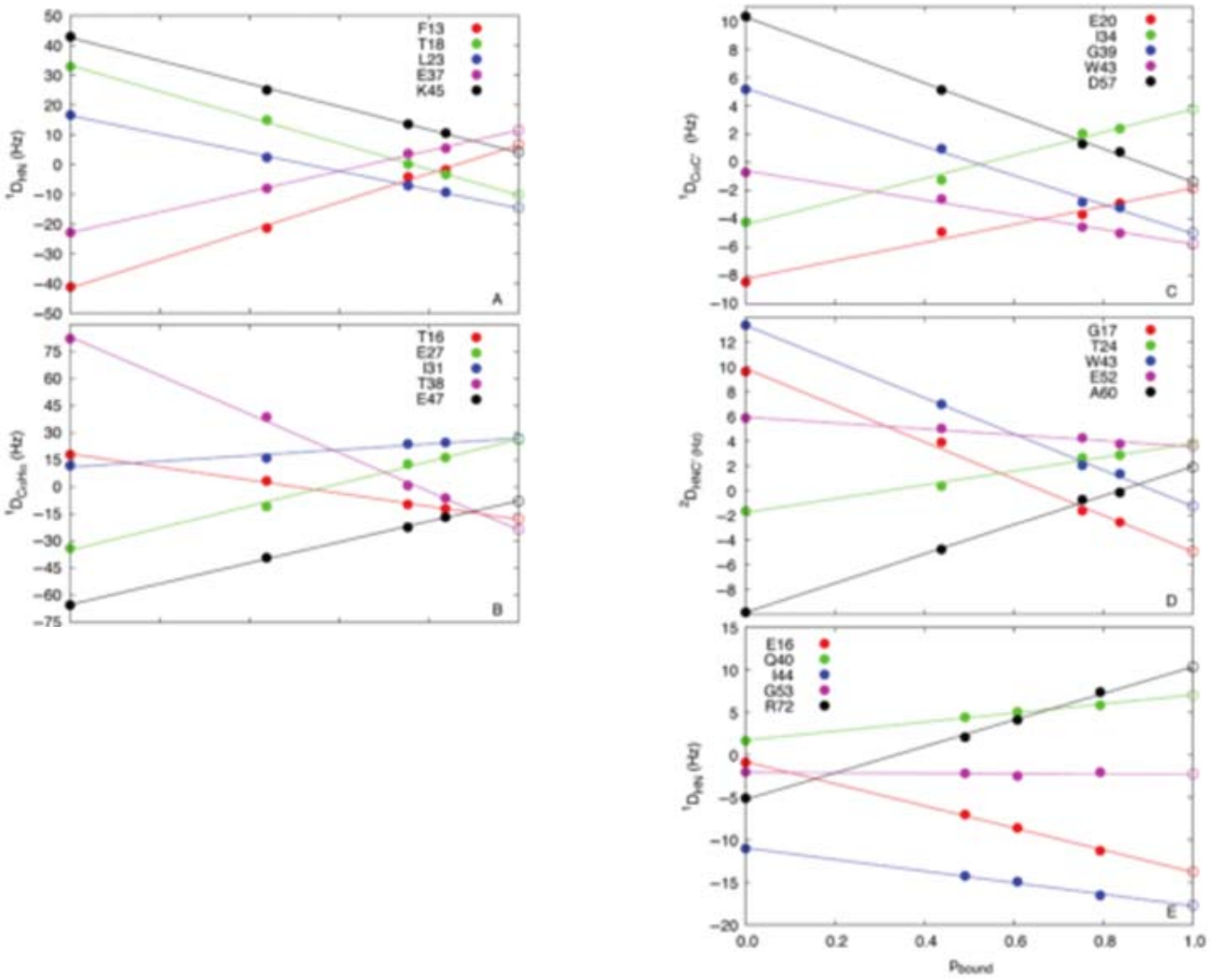

Figure 3. Plots of linearly changing RDCs with respect to population of the bound state (x-axis). The fully bound values (open circles) represent the values determined by optimization of Equation (3). The remaining values are experimental values, adjusted by optimizing the linearity of the slope by scaling the four parameters λ_1, λ_2, $\lambda_{0,ubi}$ and $\lambda_{0,sh3}$ relative to λ_3. Five sites are shown for each RDC type [(**A–D**) SH3, E Ubiquitin). The selected sites show fits of average quality.

Residual dipolar couplings (RDC)

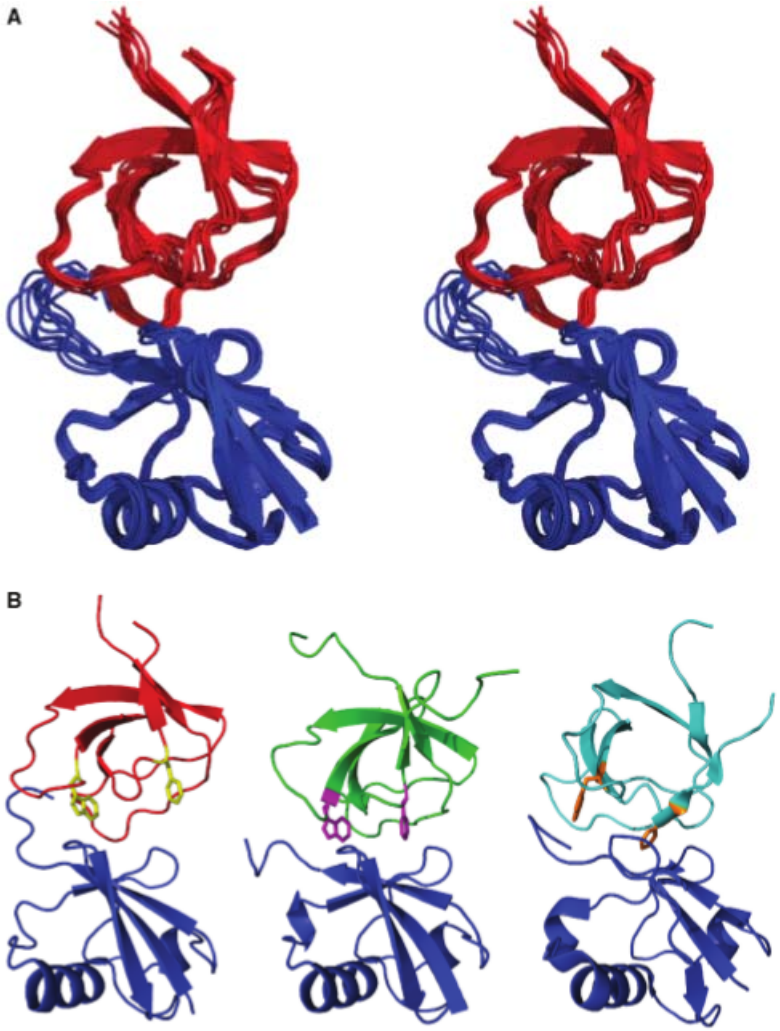

Figure 5. Structural model of the complex between CD2AP SH3-C and ubiquitin. (**A**) Stereo representation of the ensemble of 10 lowest-energy structures derived from the RDC titration protocol (SH3-C in red, ubiquitin in blue). (**B**) Comparison between the CD2AP SH3-C:Ubiquitin (SH3-C in red, ubiquitin in blue), Sla1 SH3-3:Ubiquitin complex (PDB entry 2JTA; SH3-3 in green, ubiquitin in blue) and CIN85 SH3-C:Ubiquitin (PDB entry 2K6D; SH3 in cyan, ubiquitin in blue). Trp43 and Phe59 in CD2AP SH3-C are shown in yellow sticks and the equivalent residues in Sla1 SH3-3 and CIN85 SH3-C are shown in magenta and orange sticks, respectively. The SH3:Ubiquitin complexes were superimposed on the backbone atoms of residues 4–71 of ubiquitin (RMSD of 0.74 and 1.32 Å for Sla1 and CIN85 to CD2AP, respectively).

Ortega-Roldan, J. L. et al. Accurate characterization of weak macromolecular interactions by titration of NMR residual dipolar couplings: application to the CD2AP SH3-C:ubiquitin complex. Nucleic acids research 37, e70 (2009).

Protein/ membrane interactions

http://www.ncbi.nlm.nih.gov/pmc/articles/PMC2928847/
Curr Opin Struct Biol. 2010 August; 20(4): 471–479. Non-micellar systems for solution NMR spectroscopy of membrane proteins .Thomas Raschle, Sebastian Hiller, Manuel Etzkorn, and Gerhard Wagner

http://pubs.acs.org/doi/abs/10.1021/ja907918r
J. Am. Chem. Soc., 2009, 131 (49), pp 17777–17779. Structural and Functional Characterization of the Integral Membrane Protein VDAC-1 in Lipid Bilayer Nanodiscs. Thomas Raschle, Sebastian Hiller, Tsyr-Yan Yu, Amanda J. Rice, Thomas Walz, and Gerhard Wagner

http://www.sciencemag.org/content/321/5893/1206.full
Science 29 August 2008: Vol. 321 no. 5893 pp. 1206-1210. Solution Structure of the Integral Human Membrane Protein VDAC-1 in Detergent Micelles. Sebastian Hiller, Robert G. Garces,* Thomas J. Malia, Vladislav Y. Orekhov, Marco Colombini, Gerhard Wagner

http://www.sciencedirect.com/science/article/pii/S0005273611004007
Biochim Biophys Acta. 2012 Jun;1818(6):1562-9. doi: 10.1016/j.bbamem.2011.11.012. Epub 2011 Nov 15.
Solution NMR spectroscopic characterization of human VDAC-2 in detergent micelles and lipid bilayer nanodiscs. Yu TY, Raschle T, Hiller S, Wagner G.

NMR study of the proteosome

http://onlinelibrary.wiley.com/doi/10.1002/cbic.200500110/full
Tugarinov, V. & Kay, L. E. Methyl groups as probes of structure and dynamics in NMR studies of high-molecular-weight proteins. Chembiochem : a European journal of chemical biology 6, 1567–77 (2005).

http://www.sciencemag.org/content/328/5974/98
Religa, T. L., Sprangers, R. & Kay, L. E. Dynamic regulation of archaeal proteasome gate opening as studied by TROSY NMR. Science (New York, N.Y.) 328, 98–102 (2010).

http://www.nature.com/nature/journal/v467/n7317/full/nature09444.html
Ruschak, A. M., Religa, T. L., Breuer, S., Witt, S. & Kay, L. E. The proteasome antechamber maintains substrates in an unfolded state. Nature 467, 868–71 (2010).

http://pubs.acs.org/doi/abs/10.1021/ja2014532
Hansen, D. F. & Kay, L. E. Determining valine side-chain rotamer conformations in proteins from methyl 13C chemical shifts: application to the 360 kDa half-proteasome. Journal of the American Chemical Society 133, 8272–81 (2011).

Various techniques to study macromolecular interactions

http://www.sciencedirect.com/science/article/pii/S1047847710003424
Wang, X., Lee, H.-W., Liu, Y. & Prestegard, J. H. Structural NMR of protein oligomers using hybrid methods. Journal of structural biology 173, 515–29 (2011).

http://www.sciencedirect.com/science/article/pii/S0969212611002061
Wang, X., Watson, C., Sharp, J. S., Handel, T. M. & Prestegard, J. H. Oligomeric structure of the chemokine CCL5/RANTES from NMR, MS, and SAXS data. Structure (London, England : 1993) 19, 1138–48 (2011).

http://onlinelibrary.wiley.com/doi/10.1002/pro.447/abstract
Lee, H.-W. et al. Three-dimensional structure of the weakly associated protein homodimer SeR13 using RDCs and paramagnetic surface mapping. Protein science : a publication of the Protein Society 19, 1673–85 (2010).

http://www.sciencedirect.com/science/article/pii/S0022283604011143
Jain, N. U., Wyckoff, T. J. O., Raetz, C. R. H. & Prestegard, J. H. Rapid analysis of large protein-protein complexes using NMR-derived orientational constraints: the 95 kDa complex of LpxA with acyl carrier protein. Journal of molecular biology 343, 1379–89 (2004).